PHILOSOPHICAL TRANSACTIONS OF THE ROYAL SOCIETY A MATHEMATICAL, PHYSICAL & ENGINEERING SCIENCES

Plutonic Rocks of the 1985 Tibet Geotraverse, Lhasa to Golmud

N. B. W. Harris, Xu Ronghua, C. L. Lewis and Jin Chengwei

Phil. Trans. R. Soc. Lond. A 1988 **327**, 145-168
doi: 10.1098/rsta.1988.0124

Phil. Trans. R. Soc. Lond. A **327**, 145–168 (1988) [145]
Printed in Great Britain

Plutonic rocks of the 1985 Tibet Geotraverse, Lhasa to Golmud

By N. B. W. Harris[1], Xu Ronghua[2], C. L. Lewis[1] and Jin Chengwei[2]

[1] *Department of Earth Sciences, Open University, Walton Hall, Milton Keynes MK7 6AA, U.K.*
[2] *Institute of Geology, Academia Sinica, P.O. Box 634, Beijing, People's Republic of China*

[Microfiche in pocket]

Two large east-trending granitic batholiths are exposed on the plateau of Central Tibet. In the southern Lhasa Terrane, north of the Zangbo Suture, the Gangdise Belt is a calc-alkaline composite batholith dominated by monzodiorites, tonalites, granodiorites and monzogranites. Trace elements indicate that strongly fractionated melts were emplaced at an active continental margin; deeper crustal levels of the batholith are exposed in the crustally-derived Nyainqentanglha orthogneiss. Along the northern edge of the plateau, a syn-tectonic calcic to calc-alkaline suite of tonalites, granodiorites and monzogranites forms the Kunlun batholith with post-tectonic granites emplaced to the south. The Kunlun intrusions are derived from anatexis of a garnet-bearing source at intermediate crustal depths above an active or recently active continental margin.

Between these two batholiths, a bimodal suite of metaluminous tonalite-granodiorite and peraluminous two-mica granite is exposed in the northern Lhasa Terrane, indicative of melting both in the upper crust and at deeper levels in the crust or upper mantle. This association suggests a post-collision setting.

1. Introduction

The Sino–British Geotraverse of Tibet identified three continental fragments which now comprise the Tibetan Plateau; the Lhasa, Qiangtang and Kunlun Terranes (Chang *et al.* 1986). Plutonic magmatism exposed along the route is largely restricted to three major regions; an east-trending batholith in the southern Lhasa Terrane, a broad belt of discrete plutons in the northern Lhasa Terrane and a second east-trending batholith in the Kunlun Mountains. The exposures in the Qiangtang and southern Kunlun Terranes are almost entirely restricted to volcano-sedimentary units but stream samples of granitoids suggest that a plutonic belt may be exposed along the Tanggula Shan both east and west of the Geotraverse route. This paper describes the petrology, geochemistry and petrogenesis of the three plutonic belts from south to north along the Geotraverse route.

2. Techniques and data collection

Major element analyses were determined by energy dispersive X-ray fluorescence on fusion discs at the Open University, and by wet chemical techniques at the Institute of Geology, Beijing (Academia Sinica). Trace elements (Rb, Sr, Ba, Y, Zr, Nb, Th and U) were determined by XRF analysis of pressed pellets and also by neutron activation analysis (U, Th, Ta, Hf, REE) at the Open University and computed using the methods of Potts *et al.* (1981). Trace

elements (Sr, Ba, Zr, Y, La) were determined in the Institute of Geology, Beijing (Academia Sinica) by ICP.

Selected analyses of Open University data are given in tables 1–3. The complete data-set of 110 analyses with the provenance of the data is available on microfiche (in pocket).

3. Plutonism of the southern Lhasa Terrane

(a) *The Gangdise Belt*

The southern edge of the Lhasa Terrane is intruded by a 3000 km long east-trending belt of magmatic rocks known as the Gangdise Belt, sometimes referred to as the Trans-Himalaya batholith in earlier publications. The plutonic complex is emplaced immediately north of the Zangbo Suture which defines the southern limit of the Lhasa Terrane and intrudes both its volcanic cover and folded Mesozoic sediments. The geochemistry of the belt has been the subject of numerous studies which have concentrated on four areas (figure 1); North Kohistan and Karakoram (Debon *et al.* 1987; Petterson & Windley 1985), Ladakh (Honnegar *et al.* 1982), Kailas (*ibid*) and the Lhasa–Zangbo Traverse (Debon *et al.* 1986; Jin & Xu 1980). It is the Lhasa–Zangbo Traverse which has been the area of further investigation in this study.

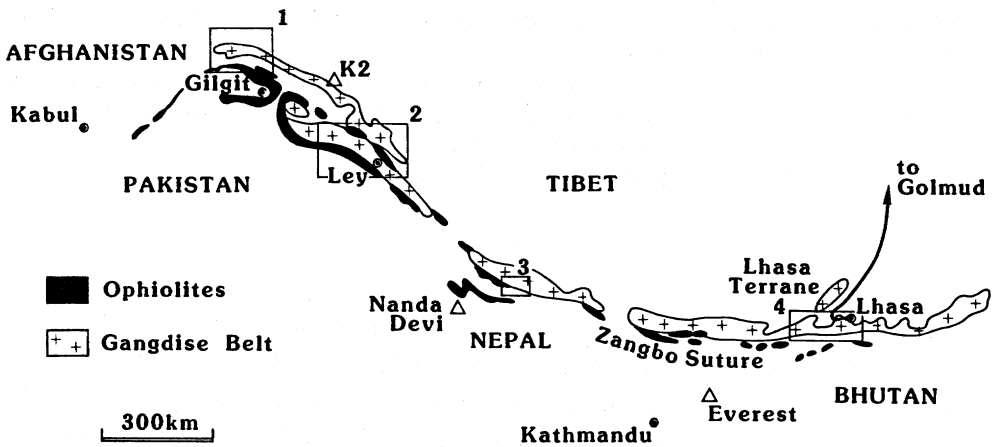

Figure 1. Sketch-map of distribution of granitoids from the Gangdise Belt intruded north of the Zangbo ophiolite. Localities of published geochemical data: 1. North Kohistan and Karakorum. 2. Ladakh. 3. Kailas. 4. Lhasa-Zangbo traverse. For references see text.

The northern limit of the Gangdise Belt to the north of Lhasa is equivocal. Previously it has been defined 30 km beyond the northern limit of the Lhasa–Gurong pluton (which lies about 50 km north of the Zangbo Suture) and includes a small granite body east of Yangbajain (Debon *et al.* 1986). In this study the belt is extended to include the extensive granitoids of the Nyainqentanglha Mountains, 10 km north-west of Yangbajain, on the basis of geochemical and isotopic similarities of these rocks with those exposed in the southern Gangdise Belt (figure 2).

(b) *Field relations and Petrology*

From the Zangbo Suture to 20 km north of Lhasa a suite of plutonic rocks emplaced into volcanics and Mesozoic sediments is known as the Quxu, Dagze and Lhasa–Gurong intrusions.

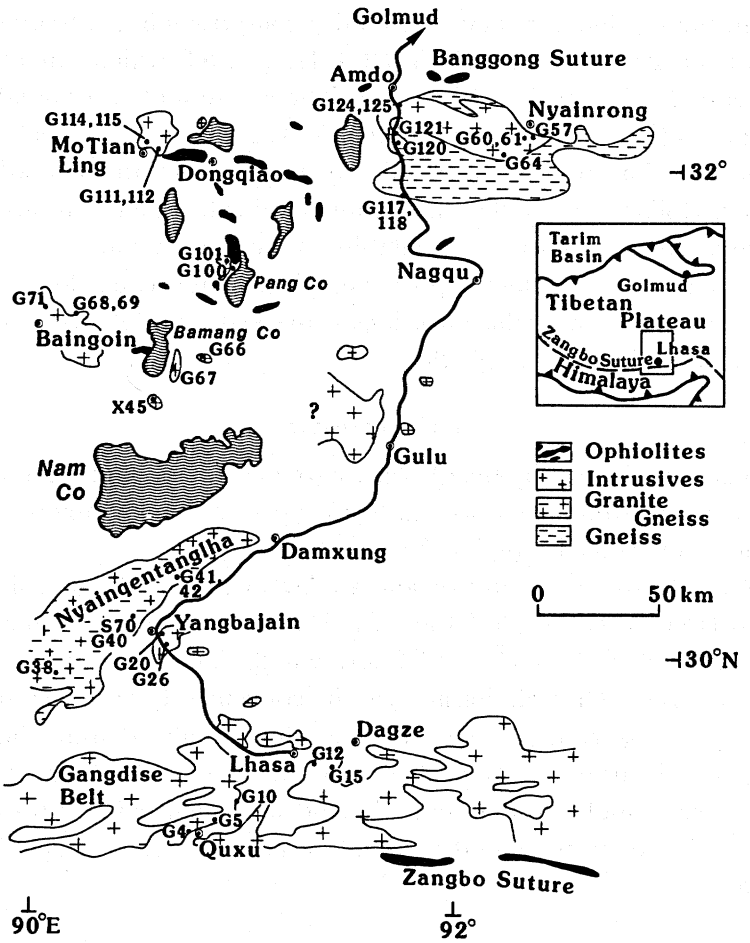

FIGURE 2. Sample location map for geochemical samples from the Lhasa Terrane.

The boundaries between these bodies are gradational and since petrological variation within any one 'intrusion' is considerable they are here described as a composite plutonic complex, representative of the southern Gangdise Belt. The igneous suite is characterized by olivine gabbro (< 5% of exposed outcrop), hornblende quartz diorite, hornblende–biotite monzodiorite (G4, G5), tonalite (G15A), biotite–hornblende granodiorite (G12) and biotite monzogranite (G10). The Streckeisen (1976) petrological classification is used throughout this study. No deformation is observed towards the core of these bodies, but a foliation is frequently developed towards their margins. Contacts with non-plutonic rocks are sharp and contact metamorphism is developed locally. For example, along the northern contact of the Lhasa body diopside and idocrase occur within Jurassic limestone and along its western margin it intrudes volcanics from the Linzizong Formation within which pinite replacement of cordierite is developed close to the contact.

The Yangbajain intrusion (6 × 10 km in outcrop area) contains two plutonic facies intruded into Carboniferous sandstone. A biotite-hornblende-sphene granite (G26) is intruded by a more leucocratic biotite granite (G20) containing large xenoliths of biotite gneiss and injection migmatites. Although no diagnostic metamorphic minerals have been found in these xenoliths, they strongly resemble pelitic gneiss exposed 20 km north in the Nyainqentanglha Mountains.

Exposures from the Nyainqentanglha Mountains comprise foliated biotite granites (G42B, S70D) and granite gneisses (G38E, G40, G41B, G42A, S70C) which extend for about 80 km along the north-east-trending strike of the range. These granitoids vary in fabric from slightly foliated to orthogneiss (but are all granites *sensu stricto*); gabbroic xenoliths have been found in some gneissic boulders. The granites have undergone upper amphibolite grade metamorphism (> 700 °C, Harris, Holland & Tindle, this volume) and subsequent retrogression resulting in chlorite, muscovite, sphene and occasional allanite. Analysis of metamorphic assemblages from xenoliths within the gneisses indicates depths of emplacement greater than 10 km. The north-eastern limit of the Nyainqentanglha intrusions is marked by a foliated two-mica granite in fault-contact with staurolite–garnet phyllites.

(*c*) *Geochemistry*

The petrological suite defined by the Quxu, Dagze and Lhasa–Gurong intrusions represent a range of silica contents from 50–73 wt. %. Rock types are metaluminous becoming slightly peraluminous for more evolved samples (SiO_2 > 70 wt. %).

There has been some discussion in previous studies about the calc-alkali characteristics of the Gangdise Belt (Debon *et al.* 1986). 'Calc-alkali' is a much used term, defined originally as a suite of rocks in which CaO = (Na_2O+K_2O), wt. %, for silica contents between 56 and 61 wt. % (Peacock 1931). This relationship can be conveniently displayed on a SiO_2 vs $\log_{10}$ ($CaO/(Na_2O+K_2O)$) diagram (Brown 1982). Samples analysed from the Zangbo–Nyainqentanglha traverse fall within the range of normal calc-alkali rocks (figure 3), and their major element geochemistry is similar to that found in Andean andesites in contrast, for example, to the High Himalaya leucogranites found south of the Zangbo Suture which lie well within the alkali-calcic field.

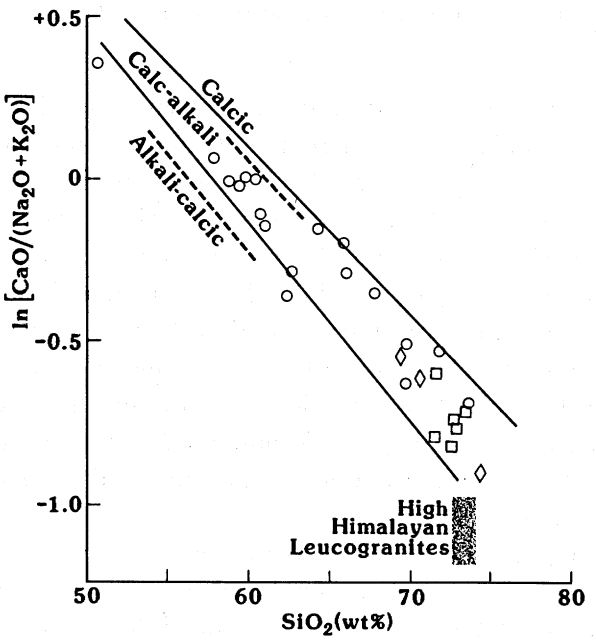

FIGURE 3. Plot of $\log_{10}(CaO/(Na_2O+K_2O))$ against SiO_2 for samples from Gangdise Belt (Zangbo–Nyainqentanglha traverse). Broken lines indicate boundaries of calc-alkali field. Solid lines define field of Andean andesites (Brown 1982). Data from Table 1 and Debon *et al.* 1986. ○ = Lhasa-Gurong-Quxu, ◇ = Yangbajain, □ = Nyainqentanglha.

Major element variation plots (figure 4) show a systematic decrease in Fe, Ca, Mg and an increase in K with silica contents. Trends of this type are an ambiguous indicator of fractionation, both because of the dilution effect of increasing SiO_2 on other major element oxides and because apparent trends could result from assimilation of a granitic end-member, but a general interpretation is that fractionating phases contain Fe, Mg and Ca, but not alkalis, such as hornblende. Amphibole fractionation would also result in the switch from metaluminous to peraluminous compositions observed in more evolved samples. However, trace element plots (figure 4) are less coherent. Rb and Sr show characteristic trends for plagioclase fractionation,

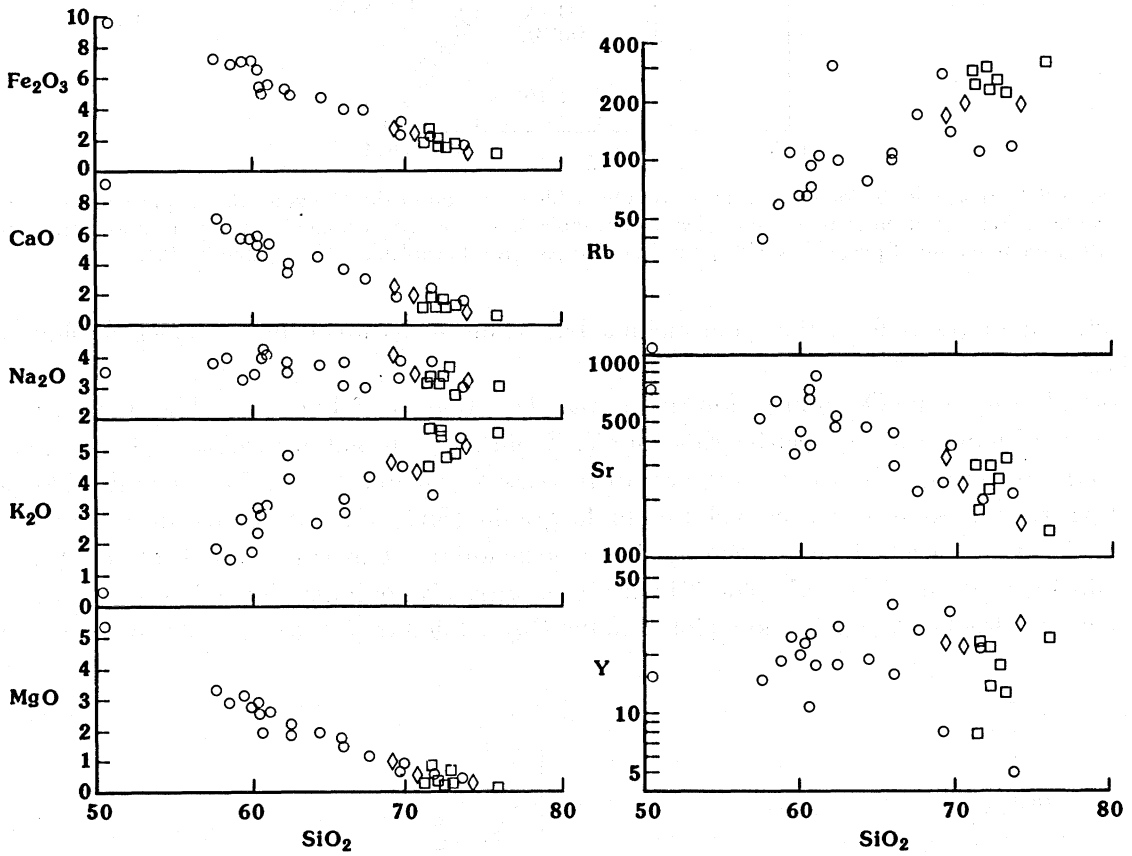

FIGURE 4. Silica variation diagrams for samples from Gangdise Belt (Zangbo-Nyainqentanglha traverse). Oxides in wt. %, trace elements in p.p.m. All Fe calculated as Fe_2O_3. Symbols and data sources as for figure 3.

but Y, a generally immobile element, shows a poor correlation with SiO_2. For $SiO_2 < 68$ wt. % there is a general increase with silica content indicating incompatible behaviour. More siliceous samples have widely ranging Y contents suggesting complex accessory phase fractionation.

To analyse the major phases responsible for fractionation within a restricted zone of the batholith, Rb/Sr vs Sr has been plotted from the Quxu–Lhasa section (figure 5). Fractionation trends for observed major phases are also plotted. This shows clearly that fractionation is controlled by feldspar rather than biotite, although hornblende fractionation would not be apparent on this plot. About 30 % feldspar fractionation is required to derive the granite (G10) from the monzodiorite (G5). However a second monzodiorite (G4), although lying close to this

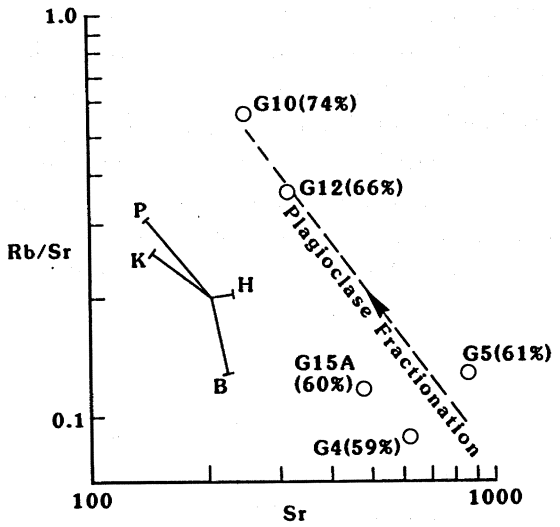

FIGURE 5. Rb/Sr against Sr for samples from the Quxu-Lhasa section of the Gangdise Belt. Approximate SiO_2 contents (wt. %) given in parentheses. Data from table 1. Vectors give change in magma composition from 10% fractionation of plagioclase (P), potassium feldspar (K), hornblende (H) and biotite (B).

trend, cannot result from the same magma batch due to its much lower K/Rb at similar SiO_2.

REE plots from the Quxu intrusion (figure 6*a*) show that the gabbro has a high LREE/HREE ratio, consistent with a garnet-bearing source. Evolution from gabbro ($SiO_2 = 51$ wt. %) to granodiorite ($SiO_2 = 62$ wt. %) require an increase in all REE except Eu – a indication of feldspar fractionation. However evolution to the granite ($SiO_2 = 70$ wt. %) requires fractionation of a HREE-enriched phase such as zircon or xenotime. This is mimicked, although less convincingly, in the SiO_2 vs Y plot of figure 4. Both trends are indicative of late-stage zircon or xenotime fractionation. The REE plot from the Dagze tonalite (G15a, figure 6*a*) indicates an

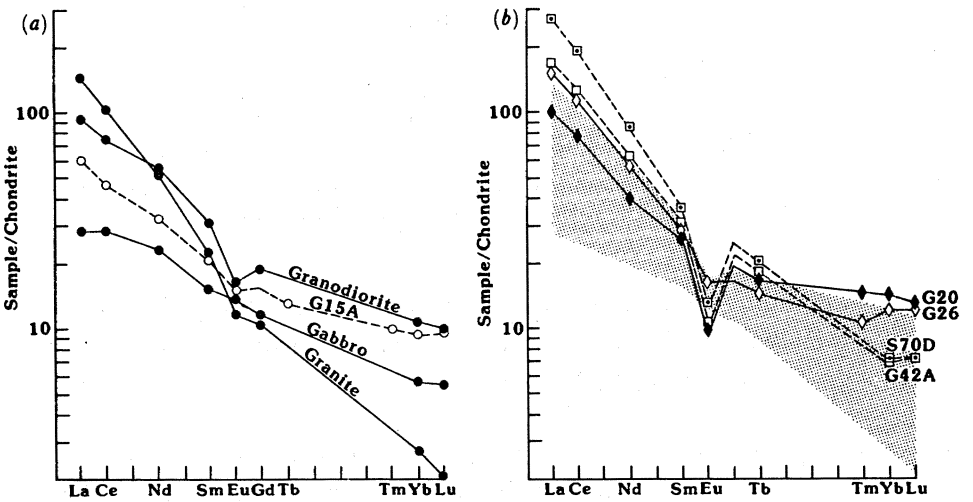

FIGURE 6. Chondrite normalized REE plots for Gangdise Belt intrusives. (*a*) solid lines indicate Quxu pluton (data from Debon *et al.* 1986). Broken line indicates Dagze tonalite (G15A). (*b*) Yangbajain granite (G20, G26), and Nyainqentanglha granite gneiss (G42A, S70D). Shaded region delineates range from Quxu intrusion. Data from table 1.

REE profile with a similar LREE/HREE to the Quxu granodiorite, but with a smaller Eu anomaly indicating a smaller degree of feldspar fractionation in the tonalitic magma.

In summary, geological evolution within the southern Gangdise Belt is dominated by feldspar and hornblende fractionation from gabbroic melts in the early stages, but also by minor phases in the more evolved samples. Isotopic constraints (Harris, Xu *et al.* this volume) require crustal assimilation to contribute to magmagenesis of tonalites and granites from the Gangdise Belt. Not all samples can be related to the same source, even within a restricted area such as Quxu.

The Rb vs (Nb+Y) and Rb vs (Ta+Yb) plots are useful indicators of tectonic setting for fresh equigranular granitic rocks (Pearce *et al.* 1984). Samples from throughout the Gangdise Belt fall within the volcanic arc/post-collision field in strong contrast to the syn-collision High Himalayan leucogranites found south of the Zangbo Suture (figure 7*a*), although since some of these samples represent the data-base from which the plots were derived, this is unsurprising. Since the publication of Pearce *et al.* (1984), it has been established that the high Rb-low HFS element field has encompassed not only syn-collision granites such as from the High Himalayas, but also post-collision crustal melts, such as the Alpine Novate intrusion (Harris *et al.* 1986). Moreover the geochemically similar Pyrenean leucogranites, although undoubtedly crustal melts, may have been generated in an extensional environment (Wickam & Oxburgh 1986). For these reasons the field has been relabelled 'upper crustal melt', which does not of course preclude granites with crustal components falling in other fields. It does however encompass those granites formed largely from melting of the upper crust due to anomalously high temperatures in that crust whether these are induced by collision or crustal thinning.

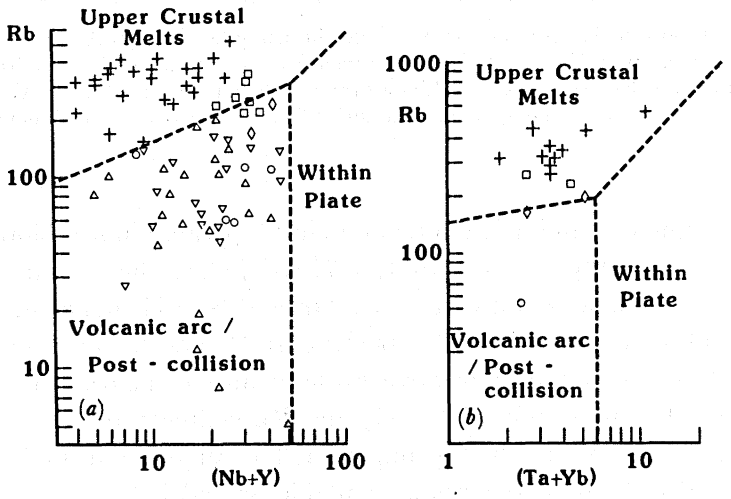

FIGURE 7. (*a*) Rb vs (Nb+Y) plot (*b*) Rb vs (Ta+Yb) plot for samples from Gangdise Belt and High Himalaya leucogranites (+, data from Dietrich & Gansser 1981, Harris *et al.* 1986). △ = Kohistan, ▽ = Ladakh. Other symbols as for figure 3. Field boundaries from Pearce *et al.* (1984).

The Yangbajain body is a metaluminous biotite–hornblende–sphene monzogranite intruded by peraluminous biotite granite. The metaluminous phase is indistinguishable from the granites exposed in the Lhasa–Quxu region to the south in both major and trace element plots. It is part of the calc-alkaline trend (figure 3), has a similar REE profile to the Quxu granodiorite (sample G26, figure 6*b*) and lies in the volcanic arc field in the tectonic discrimination diagrams (figure

7*a*, *b*). Spidergram plots of a range of trace elements (figure 8) indicates that the granite is virtually identical to Andean continental margin granites of similar SiO_2 contents. The younger peraluminous granite is more depleted in Eu than samples from the southern Gangdise Belt (sample G20, figure 6*b*) which implies either a small degree partial melt of feldspar-bearing source rock, or plagioclase fractionation.

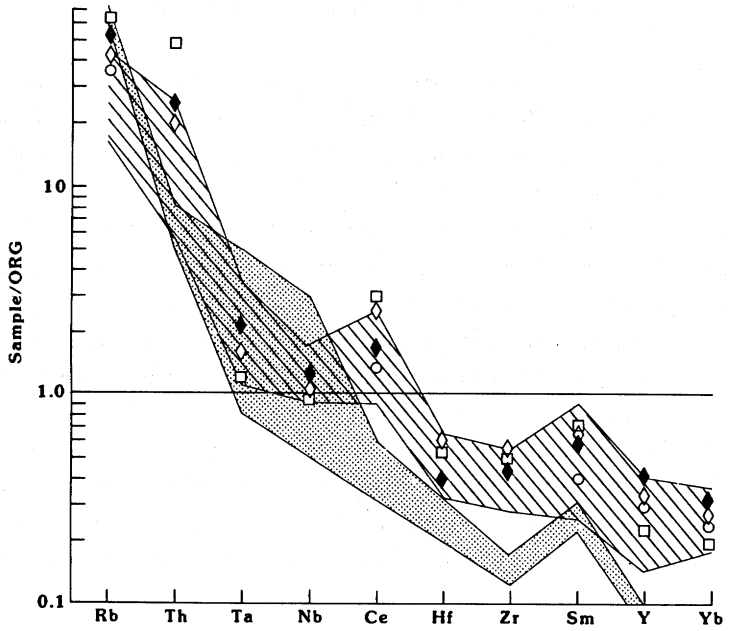

FIGURE 8. Geochemical patterns for granitic samples from the Gangdise Belt (SiO_2 = 68–75 wt. %) normalized against Ocean Ridge Granite (Pearce *et al.* 1984). Lined field = volcanic arc/post-collision granites, stippled field = High Himalayan leucogranites. ○ = Lhasa granite (Debon *et al.* 1986), ◇ = G26 (Yangbajain, metaluminous facies), ◆ = G20 (Yangbajain peraluminous facies), □ = S70D (Nyainqentanglha). Data from table 1.

The Nyainqentanglha samples are predominantly peraluminous biotite syeno-monzogranites. They are all highly evolved (SiO_2 > 71 wt %) and lie within a calc-alkali field (figure 3). They have somewhat lower Fe, Ca, Mg and Sr and higher K and Rb than the calc-alkaline rocks of the southern Gangdise belt (figure 4). The Nyainqentanglha samples are also LREE-enriched and show larger negative Eu anomalies compared to southern Gangdise samples (figure 6*b*). The uniformly high SiO_2 and Rb contents and strongly peraluminous compositions from samples across the Nyainqentanglha range are an indication that crustal melting was involved in their petrogenesis. Available Sr and Nd isotopic data (Harris, Xu, Lewis, Hawkesworth & Zhang, this volume) require a crustal source and preclude an origin by simple fractionation of amphibole and feldspar from calc-alkaline magmas now represented in the southern Gangdise Belt.

In the Rb vs (Nb+Y) plot (figure 7*a*) Nyainqentanglha samples straddle the volcanic arc/post collision and crustal melt fields. These granites however differ from crustal melts derived from collision-related anatexis such as the High Himalaya leucogranites (figure 8) in their much higher Th and LREE contents and their smaller depletions in HFS elements (Hf, REE, Y). Th enrichment in subduction-related magmas may be interpreted as a

component from subducted sediments (Pearce 1982) but Th contents in the Nyainqentanglha granites (28–78 p.p.m.) are much higher than those observed in magmatic arcs (< 20 p.p.m. Brown *et al.* 1984). U, with the exception of S70C which is a highly evolved granite (SiO_2 > 76 wt. %), is not enriched in the Nyainqentanglha granites. Th and LREE bearing phases observed in the granites include allanite and monazite.

The high Th and LREE contents of the Nyainqentanglha granites result from either late-stage accessory phase crystallization from the magma or entrainment of these phases into the magma from the source rock during anatexis, a process inferred from studies of other crustally-derived granites (Sawka *et al.* 1986). Microprobe studies of accessory phases are required to identify the dominant host phase of Th and LREE, but the discordant nature of some zircons from the granites provides evidence that this phase at least is inherited from the source region (Xu *et al.* 1985).

TABLE 1. SELECTED ANALYSES FROM SOUTHERN LHASA TERRANE

	Quxu		Lhasa		Dagze	Yangbajain		Nyainqentanglha		
	G4	G5	G10	G12	G15A	G20	G26	G42A	S70C	S70D
	MzD	MzD	Gr	Gd	Ton	Gr	Gr	Gr gn	Gr gn	Gr
SiO_2	58.73	61.00	73.76	65.96	60.00	74.25	69.30	72.23	76.05	72.87
TiO_2	0.71	0.70	0.22	0.75	0.83	0.19	0.43	0.31	0.11	0.26
Al_2O_3	17.18	16.85	14.20	15.41	16.86	14.14	15.77	15.46	13.75	14.52
Fe_2O_3	6.97	5.61	1.73	4.98	7.24	1.31	2.99	2.06	1.25	1.79
MnO	0.13	0.10	0.03	0.07	0.14	0.08	0.09	0.03	0.02	0.04
MgO	2.82	2.63	0.61	1.56	2.80	0.12	0.98	0.39	0.18	0.31
CaO	6.15	5.34	1.71	4.17	5.74	1.02	2.54	1.64	0.89	1.44
Na_2O	3.99	4.25	3.00	3.44	3.92	3.43	4.20	3.60	3.29	3.67
K_2O	2.55	3.27	5.53	3.16	1.84	5.18	4.66	5.53	5.71	4.81
P_2O_5	0.20	0.28	0.05	0.18	0.23	0.00	0.15	0.08	0.13	0.08
LOI	0.35	0.32	0.21	0.61	0.33	0.21	0.51	0.26	0.37	0.33
Total	99.78	100.35	101.05	100.29	99.93	99.93	101.63	101.59	101.75	100.12
ppm										
Rb	58	110	137	108	57	229	174	236	339	264
Sr	645	867	242	304	470	152	368	303	127	236
Ba	623	660	370	620	381	358	880	330	< 210	750
Zr	127	174	99	208	101	119	190	225	118	175
Hf	—	—	—	—	3.9	3.8	5.5	6.9	—	5.3
Nb	6	13	3	7	7	13	10	8	17	10
Ta	—	—	—	—	0.44	1.6	1.2	3.0	—	0.92
Y	19	18	5	36	20	30	24	14	25	18
Th	6	27	21	6	4.0	21	17	7.3	55	43
U	< 3	6	4	< 3	1.0	3.0	3.4	8.9	31	6.3
La	—	—	—	—	21	34	53	90	—	54
Ce	—	—	—	—	41	69	101	167	—	108
Nd	—	—	14	—	21	26	36	54	38	38
Sm	—	—	1.7	—	4.3	5.6	6	7.2	8.1	6.3
Eu	—	—	—	—	1.2	0.77	1.3	1.0	—	0.83
Tb	—	—	—	—	0.68	0.89	0.75	1.1	—	0.95
Tm	—	—	—	—	0.34	0.52	0.36	—	—	—
Yb	—	—	—	—	2.1	3.3	2.8	1.5	—	1.6
Lu	—	—	—	—	0.34	0.46	0.42	0.25	—	0.25

MzD = monzodiorite, Gr = granite, Gd = granodiorite, Ton = tonalite, gn = gneiss.

PHILOSOPHICAL TRANSACTIONS OF THE ROYAL SOCIETY A MATHEMATICAL, PHYSICAL & ENGINEERING SCIENCES

4. Plutonism of the northern Lhasa Terrane

(a) *Field relations and petrology*

Between the Nyainqentanglha Belt and the Banggong Suture lies a 100 km wide east-trending belt of predominantly intrusive magmatism (figure 2). The intrusions display pre-kinematic fabric such as foliated margins or elliptical cordierite spots in the contact zones although many of the samples appear undeformed in outcrop.

The best exposed pluton in the belt outcrops south-east of Baingoin and is a composite body which comprises a biotite tonalite (G68) intruded by a two-mica tourmaline granite (G69, G71) with tonalite enclaves and cut by tourmaline-muscovite pegmatites. Contacts between the intrusion and the Carboniferous shales it intrudes are semi-concordant and within the metasediments a narrow garnet–tourmaline–topaz aureole is developed.

On the north-west banks of Pung Co, biotite granite (G100) is intrusive into both Jurassic sediments and a 1 km diameter plug of hornblende–hypersthene–biotite granodiorite (G101). Both intrusions post-date allochthonous gabbros associated with a dismembered sliver of Banggong ophiolite. A similar association of biotite granites and granodiorite–quartz monzonite is emplaced to the south-east of Bamang Co (G67, X45).

The largest known outcrop of intrusive rock in the northern Lhasa Terrane is the Nyainrong–Amdo batholith which covers an area at least 2000 km^2 south-east of Amdo. Exposed along the Nagqu–Nyainrong road, the dominant rock-type is a porphyritic biotite granite (G64), within which patches of strongly porphyritic (5–10 cm microcline megacrysts) hornblende–biotite granite are developed (G60, G61). The intrusion is transected by screens of biotite or hornblende gneiss and calc-silicates. Contact metamorphic skarns are observed in the calc-silicates containing diopside and idocrase. South of Amdo a biotite–hornblende granodiorite (G124) is locally strongly porphyritic and intrudes both amphibolite (G117) and biotite orthogneiss (G118).

Twenty kilometres north-west of Dongqiao, near Mo Tian Ling, Carboniferous shales are intruded by a 12 km diameter intrusion of biotite–hornblende–augite–sphene granodiorite (G111, G115) and biotite granite (G114). Regional structures indicate the Banggong Suture lies to the north of this intrusion which implies that the Mo Tian Ling pluton should be grouped with the intrusions of the northern Lhasa Terrane.

(b) *Geochemistry*

The northern Lhasa Terrane granitoids are characterized by a bimodal association of a peraluminous granite intruding a metaluminous granodiorite or tonalite. This relationship is exemplified at Baingoin by a biotite tonalite of strongly calcic geochemistry (figure 9) being intruded by a calc-alkaline peraluminous syeno-monzogranite. The high Rb and SiO_2 contents and strongly peraluminous character of the granite are indicative of a crustal component and the strong negative Eu anomaly (figure 10*a*) suggests a feldspar-bearing source. The associated tonalite (G68A) has a similar negative Eu anomaly which precludes fractionation of feldspar from the tonalite to generate the peraluminous granite. The Rb vs (Nb+Y) and Rb vs (Ta+Yb) plots (figure 11) indicate that the more calcic phase of the bimodal association lies in the volcanic arc/post-collision field whereas the peraluminous granite lies in the crustal melt field. On trace element grounds it has not been possible to distinguish 'volcanic arc' from some 'post-collision' intrusions. For example, most post-collision Alpine intrusions plot within

the volcanic arc field of figure 11. However the spatial and temporal association of 'volcanic arc' magmas and upper crustal melts is indicative of post-collision magmatism. In general, the 'volcanic arc' component is thought to be derived from near the base of the thickened crust in response to the transient geotherm and to rising mantle melts above the now defunct subduction zone (Harris *et al.* 1986). The crustal melts result from anatexis of the tectonically thickened crust in response to rising aqueous fluids from underthrust sediments. The abundance of tourmaline in many such granites suggests marine sediments as a possible boron source.

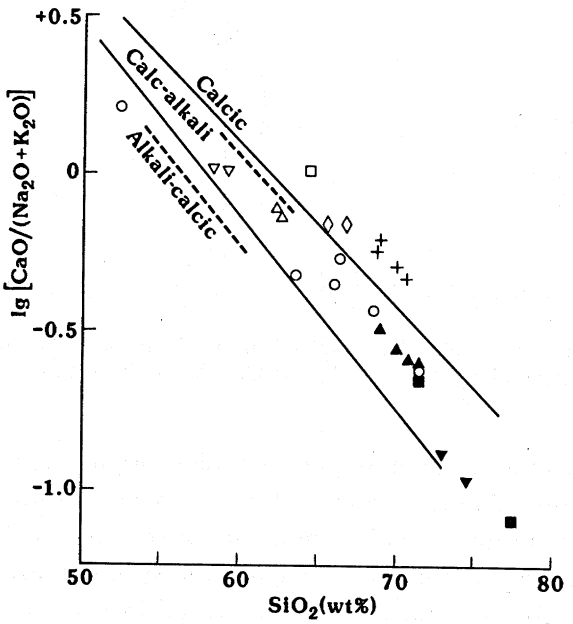

FIGURE 9. Plot of $\log_{10}(CaO/(Na_2O+K_2O))$ against SiO_2 for samples from northern Lhasa Terrane. Field boundaries as for figure 3. Data from table 2. ■ = Baingoin (granite), □ = Baingoin (tonalite), ▼ = Pung Co (granite), ▽ = Pung Co (granodiorite), ◇ = Bamang Co, ▲ = Nyainrong, △ = Amdo, ○ = Mo Tian Ling, + = basement south of Amdo.

The detailed geochemistry of the peraluminous granite however (figure 12) is distinct from the syn-collision melts of the High Himalayas. Like the Nyainqentanglha granites, Th and LREE are strongly enriched but HFS elements are only slightly depleted. These may be interpreted in one of two ways: either the magma contains a LIL-enriched component derived from the hydrated mantle wedge beneath the collision zone or the magma results from crustal anatexis under conditions where Th and LREE enter the melt. Since Th enrichment is more marked than for normal arc-related granites, and since Th enrichment is seen in the Eocene Nyainqentanglha intrusions to the south, it seems likely that the latter reason is appropriate and the Th is therefore probably crustally derived. However unlike the discordant zircons from the Nyainqentanglha gneiss, zircons and monazites of Cretaceous age from the Baingoin granite (121 ± 2 Ma) are virtually concordant (Xu *et al.* 1985). Preliminary microprobe analysis of accessory phases indicate that Th and LREE are concentrated in monazite ($ThO_2 = 6.3\%$, $Ce_2O_3 = 28.5\%$); other accessories include apatite, zircon and ilmenite. The refractory nature of monazite is critically dependent on the size of the crystals in the source rock and the water activity in the melt. For example at temperatures of 700–800 °C and under

hydrous conditions small monazites will be digested in the melt but larger crystals are residual (Rapp & Watson 1986). The concordant nature of the Baingoin monazites and zircons suggests crystallisation from the Cretaceous melt.

The Bamang Co intrusions have a higher alkali feldspar content than the Baingoin tonalite, but otherwise are geochemically similar; they are calcic rather than calc-alkaline (figure 9),

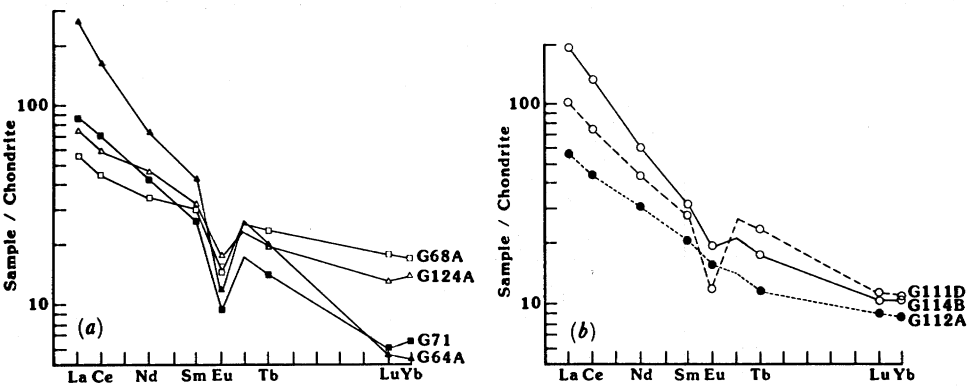

FIGURE 10. Chondrite normalized REE plots for samples from northern Lhasa Terrane. (*a*) Baingoin (G68A, G71) and Nyainrong-Amdo batholith (G64A, G124A). (*b*) Mo Tian Ling. Data from table 2.

and trace elements indicate a volcanic arc/post-collision origin (figure 11*a*). The two components of the Pung Co intrusion also show a close geochemical similarity to those from the Baingoin body. The granodiorite is metaluminous with a volcanic-arc/post-collision signature (figure 11*a*). The granite is peraluminous bridging the syeno-monzogranite boundary and trace elements (elevated Rb/HFS ratios) indicate a crustal melt origin.

The Nyainrong–Amdo batholith again reflects this bimodal association. The Amdo region is characterized by metaluminous, calc-alkaline granodiorite with trace elements indicating volcanic arc/post-collision field. Rare earth elements show a large LREE/HREE ratio and a strong negative Eu anomaly closely paralleling that of the Baingoin tonalite (G124A,

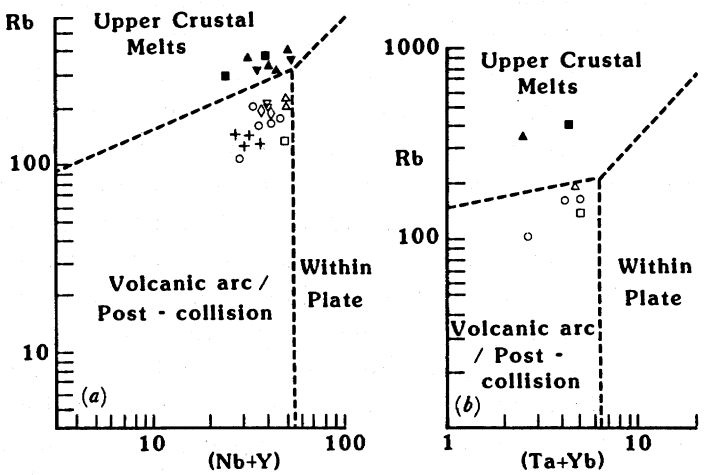

FIGURE 11. (a) Rb vs (Nb+Y) plot, (b) Rb vs (Ta+Yb) plot for samples from the northern Lhasa Terrane. Symbols as for figure 9. Field boundaries from Pearce *et al.* (1984).

figure 10). In the Nyainrong region a peraluminous monzogranite is rimmed by a metaluminous orthoclase–porphyritic monzogranite, both facies indicating a crustal melt origin (figure 11), although in the case of the strongly porphyritic phase this is inconclusive because alkalis have certainly been affected by post-crystallisation fluid mobility. The equigranular phase has trace elements similar to the Baingoin granite (figure 12) except that Th and LREE are even more enriched in the Amdo sample. Microprobe analysis of accessory phases indicate that the hosts for Th and LREE include allanite ($ThO_2 = 8.8\%$, $Ce_2O_3 = 13.8\%$) and thorite ($ThO_2 = 63.0\%$).

The exposures of basement to the south of Amdo are predominantly tonalitic orthogneiss which the Nyainrong–Amdo batholith intrudes. The orthogneiss is calcic (figure 9) and lies in the volcanic arc field of figure 11*a*. Both Rb and Th are low indicative of an island arc, rather than an active continental margin. Low Th values make this gneiss an unlikely source for the crustal melt granites of the region, and this inference is supported by isotopic arguments (Harris, Xu, Lewis, Hawkesworth & Zhang, this volume).

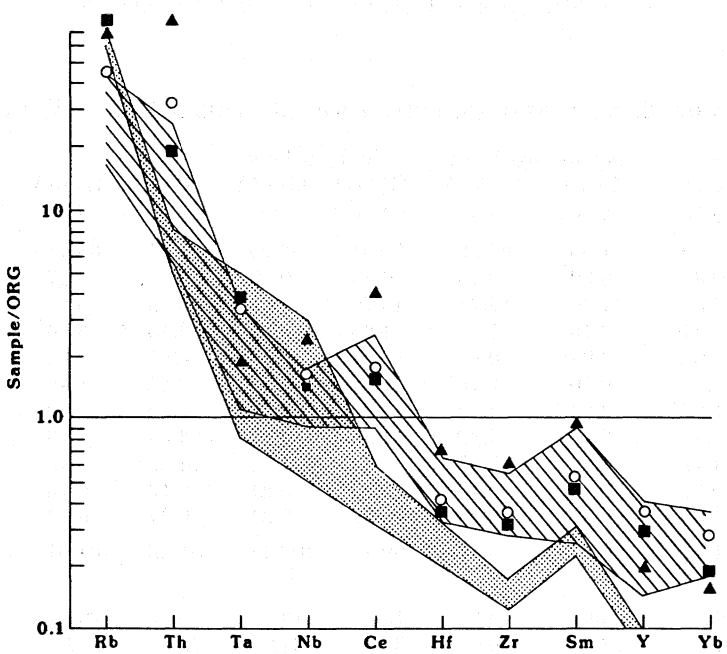

FIGURE 12. Geochemical patterns for granitic samples from the northern Lhasa Terrane ($SiO_2 = 68$–75 wt. %) normalised against Ocean Ridge Granite (Pearce *et al.* 1984). Lined field = volcanic-arc/post-collision granites, stippled field = High Himalaytan leucogranites. ■ = G71 (Baingoin), ▲ = G64A (Nyainrong), ○ = G114B (Mo Tian Ling).

The Mo Tian Ling intrusion is a granodiorite-granite which is calc-alkaline (figure 9) and lies well within the 'volcanic arc/post-collision' field of figure 11. The granodiorite (G111D) could be derived from a diorite source (G112A) since the strong negative Eu anomaly and increased REE contents of the granodiorite indicate feldspar fractionation (figure 10*b*). However, the monzogranite (G114B) has a much smaller Eu anomaly than the granodiorite, and, although the steeper LREE/HREE ratios could be modelled by fractionating a HREE-rich accessory phase such as zircon or xenotime, it is not possible to reduce substantially a negative Eu anomaly unless the granite incorporates cumulate feldspar. Therefore the REE plots

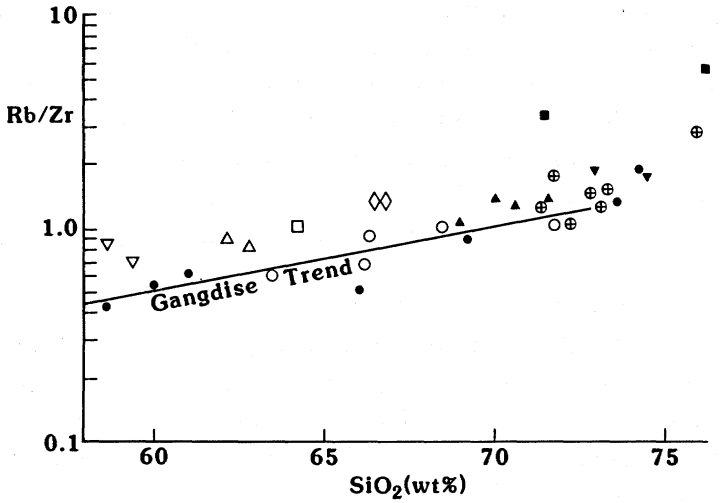

FIGURE 13. Rb/Zr vs SiO_2 for samples from the northern Lhasa Terrane compared with the Gangdise Belt (●) and the Nyainqentanglha (⊕). Other symbols as for figure 9.

TABLE 2. SELECTED ANALYSES FROM NORTHERN LHASA TERRANE

	Baingoin		Nyainrong-Amdo		Mo Tian Ling				Amdo Basement	
	G68A	G71	G64A	G124A	G111D	G112A	G114B	G115A	G118A	G118D
	Ton	Gr	por Gr	Gd	Gd	D	Gr	Gd	Ton gn	Ton gn
SiO_2	64.27	71.49	71.56	62.28	63.54	52.23	71.77	68.43	68.98	69.91
TiO_2	0.53	0.32	0.39	0.79	0.80	0.90	0.40	0.57	0.43	0.41
Al_2O_3	16.62	15.57	14.76	16.74	16.79	14.90	15.15	15.99	14.86	15.34
Fe_2O_3	5.19	3.24	2.16	5.49	4.25	8.22	2.15	3.16	4.53	3.87
MnO	0.10	0.07	0.04	0.09	0.07	0.13	0.04	0.06	0.08	0.08
MgO	2.43	1.08	0.50	2.76	1.88	8.73	0.85	1.49	1.47	1.25
CaO	5.21	1.63	2.02	4.42	3.80	7.79	2.06	2.93	3.30	3.05
Na_2O	2.55	2.85	3.28	3.89	4.35	2.83	3.65	4.06	3.74	4.39
K_2O	2.34	4.41	4.89	3.07	3.47	1.86	4.82	3.75	1.54	1.39
P_2O_5	0.13	0.17	0.10	0.16	0.23	0.21	0.13	0.16	0.10	0.08
LOI	0.75	0.88	0.57	0.88	0.59	2.34	0.34	0.47	0.76	0.39
Total	100.12	101.71	100.27	100.57	99.77	100.14	101.36	101.07	99.79	100.16
ppm										
Rb	130	391	353	198	156	103	156	201	140	129
Sr	301	112	227	262	387	311	223	287	168	137
Ba	< 310	< 270	< 280	450	580	780	320	340	410	< 280
Zr	126	119	246	212	255	116	145	171	156	137
Hf	4.2	3.7	6.8	6.7	5.9	2.9	3.8	—	—	—
Nb	10	16	19	16	18	9	16	16	11	14
Ta	0.98	2.7	1.3	1.7	1.5	0.60	2.5	—	—	—
Y	42	21	14	35	25	21	28	24	22	23
Th	7.3	17	81	14	27	5.8	37	26	17	14
U	3.1	2.9	7	7	3.2	1.1	2.4	< 4	< 3	< 3
La	19	29	90	25	64	19	34	—	—	—
Ce	40	61	147	52	114	39	65	—	—	—
Nd	23	27	48	29	39	20	29	—	34	22
Sm	6.2	5.4	9.2	6.6	6.5	4.3	5.9	—	5.7	4.5
Eu	1.1	0.74	0.97	1.4	1.5	1.2	0.93	—	—	—
Tb	1.2	0.75	1.1	1.0	0.92	0.61	1.2	—	—	—
Tm	—	—	—	—	—	—	—	—	—	—
Yb	3.9	1.4	1.3	2.9	2.4	2.0	2.5	—	—	—
Lu	0.58	0.23	0.19	0.49	0.38	0.30	0.38	—	—	—

Ton = tonalite, Gr = granite, Gd = grandiorite, D = diorite, gn = gneiss, por = porphyritic.

PHILOSOPHICAL TRANSACTIONS OF THE ROYAL SOCIETY A MATHEMATICAL, PHYSICAL & ENGINEERING SCIENCES

preclude simple fractionation from a single parent magma. The range of trace elements (figure 12) indicates a typical active continental margin or post-collision intrusion with some Th enrichment.

The high crustal component present in some post-collision magmas can not readily be demonstrated by trace elements in the absence of isotopic data. However, Rb/Zr has been used as an indicator of crustal melting (Harris *et al.* 1986), although its usefulness depends on zircon being residual during anatexis. This ratio does show that for virtually all northern Lhasa Terrane intrusives there is a shift to higher Rb/Zr for given SiO_2 contents relative to the Gangdise samples (figure 13). This may reflect the high contribution of crust found in post-collision magmagenesis compared with active continental margin processes.

In summary the northern Lhasa Terrane plutons are essentially bimodal and the two phases cannot be easily related in terms of single petrogenetic process. The earlier phase is a metaluminous, often calcic, tonalite or granodiorite. Geochemically, this phase is characteristic of an active continental margin although Rb/Zr ratios are somewhat higher. The subsequent phase is a peraluminous granite, commonly containing two micas and tourmaline. Although mineralogically similar to upper crustal melts such as the High Himalaya leucogranites, they differ geochemically in their strong Th enrichment and less-marked depletion in HFS elements. These characteristics may indicate more extensive anatexis such that accessory phases like zircon or monazite are not residual in the source rock. The association between the two distinct magma-types implies a post-collision environment in which early melts are derived from near the base of a thickened crust with crustal assimilation occurring during ascent whereas the younger melts have a predominantly upper crustal source in response to tectonic thickening.

5. Plutonism of the Qiangtang–southern Kunlun Terranes

(*a*) *Field relations and petrology*

The boundary between the Qiangtang and Kunlun Terranes is marked by the southern limit of Triassic shales south of the Kunlun Mountains, which roughly coincides with an east–west line through an ultramafic/gabbro complex to the west of the Geotraverse route (Chang *et al.* 1986). This boundary represents the Jinsha Suture marking a former northward-dipping subduction zone, the polarity being determined from the south-facing recumbency of the structures and Jurassic molasse, derived from the north, deposited south of the suture. From the Banggong Suture (which marks the southern limit of the Qiangtang Terrane), north to the Kunlun Mountains, a distance of about 500 km, there is little evidence of intrusive magmatic activity (figure 14). North of the Tanggula Pass, numerous stream samples of hornblende–hypersthene–biotite quartz monzodiorite and biotite granite (G136) have been found from an easterly source (Mt. Munai) and similar samples have been located from a westerly source in the Tuotuo River. It can be concluded that at least a small proportion of the Tanggula Mountains is underlain by granitic rocks of unknown age, but these are not exposed *in situ* along the Geotraverse route.

A small plug of phlogopite quartz microsyenite (2×1 km) is emplaced into late Cretaceous or early Tertiary sandstones of the Fenghuoshan Group in the north of the Qiangtang Terrane (G141). Fifteen kilometres south of Wudaoliang a small (3×1 km) hornblende–biotite tonalite is intruded into Triassic shales (G142). This tonalite is post-tectonic and homogeneous except for occasional dykes of peraluminous biotite granite (G143).

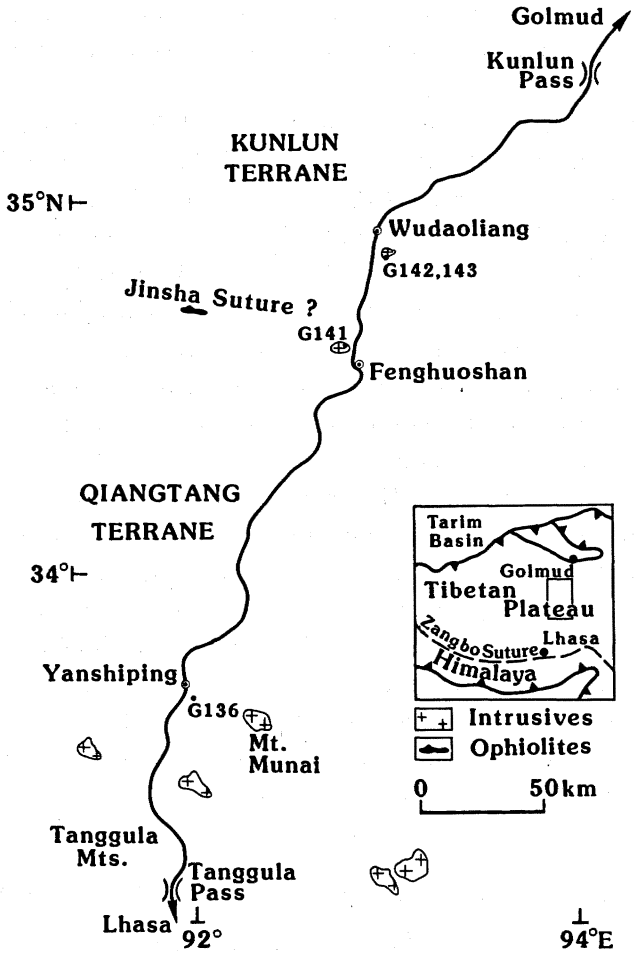

FIGURE 14. Sample location map for geochemical samples from the Qiangtang and southern Kunlun terranes.

(*b*) *Geochemistry*

The Fenghuoshan quartz microsyenite is a metaluminous alkalic body. This isolated plug intrudes Tertiary strata and must clearly be 'within plate' in tectonic setting in that no plate margin is known to be active in post-Cretaceous times within 1000 km of its emplacement. HFS element enrichment is a consistent indicator of within-plate sources, and its absence in the microsyenite may result from emplacement into anomalously thick continental crust which caused contamination by crustal melts with low HFS element concentrations. Crustal contamination is also supported by oxygen isotope data (Harris, Xu, Lewis, Hawkesworth & Zhang, this volume).

This Wudaoliang metaluminous tonalite is strongly calcic in composition. The calcic major element composition and arc-related trace element characteristics are shared by intrusions from the massive batholith of the Kunlun Mountains to the north. The Wudaoliang body represents a small post-tectonic pulse of magmatism emplaced into the accretionary prism north of the Jinsha Suture.

6. Plutonic magmatism of the Kunlun Mountains

(a) *Field relations and petrology*

The northern edge of the Tibetan Plateau is marked by the Kunlun Mountains which form an east-trending belt divided along the route of the geotraverse into a northern and southern range by the Xidatan Fault (figure 15).

Few plutonic bodies have been found intruding the Triassic phyllonites of the southern range of the Kunlun Mountains, south of the Xidatan fault. Five kilometres north of the Kunlun Pass, stream samples of granitoids include foliated two-mica granite, biotite granodiorite, hornblende–biotite quartz monzonite, hornblende diorite and pyroxenite (G204). Scree outcrops of foliated granitoids can be traced east along the ridge of the southern Kunlun. Numerous plugs or sills of post-tectonic plagioclase–quartz ± garnet porphyry have been located intruding shales on the northern slopes of the south Kunlun range.

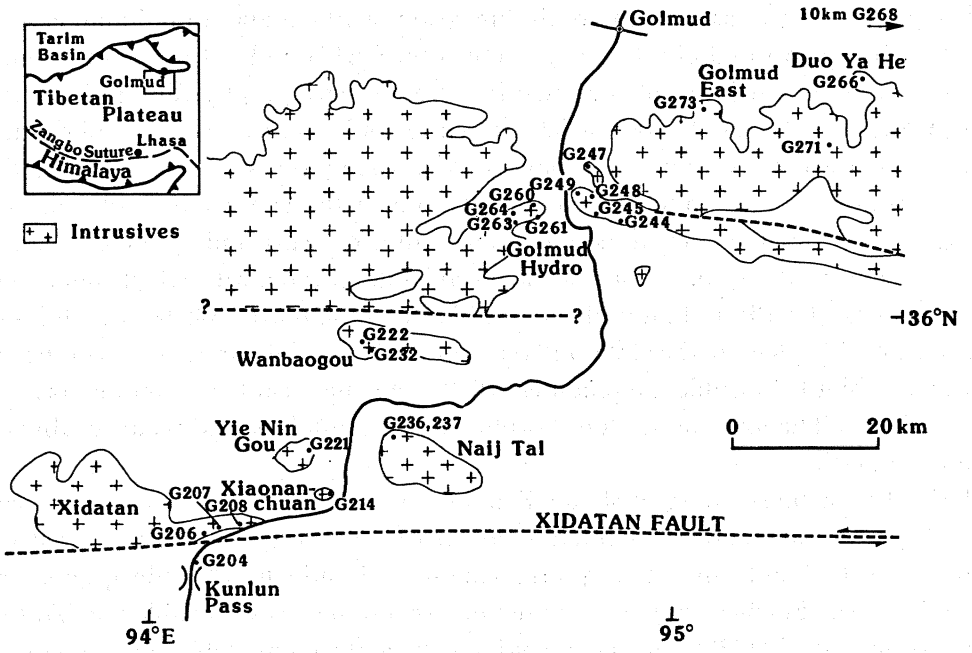

FIGURE 15. Sample location map for geochemical samples from the Kunlun Mountains.

Immediately north of the Xidatan Fault an orthogneiss is emplaced into phyllites with a strong penetrative fabric, parallel to the east-trending Xidatan Fault. The dominant rock-type is a porphyritic biotite granite gneiss (G206 A, B, G207, G208) interlayered with bands of a more leucocratic granite gneiss (G206 C, D, E). The Xidatan orthogneiss becomes weakly foliated to non-foliated as it is traced westwards.

Two kilometres north of the Xidatan Valley, west of the Lhasa–Golmud Highway, a small (2.5 km diameter) undeformed circular pluton intrudes phyllites. The intrusion, known as the Xiaonanchuan pluton (G214), is a high level post-tectonic granitoid with sharp contacts along which cordierite-bearing hornfels is developed. The pluton is a homogeneous and undeformed biotite ± sphene granite–granodiorite. A similar but larger intrusion, located 4 km north-west of the Xiaonanchuan pluton (Yie Nin Gou), is a homogeneous biotite–sphene granodiorite (G221) containing biotite-rich autoliths and calc-silicate xenoliths.

The third and largest intrusion in this group of post-tectonic granites is emplaced south-west of Naij Tal. The Naij Tal intrusion is a 20×10 km body of biotite $\pm$ hornblende granite–granodiorite (G236, G237) with limestone xenoliths and dioritic enclaves. It is emplaced into limestones and shales and a sub-horizontal upper contact indicates that the intrusion is exposed close to the roof of the magma chamber.

Fourteen kilometres north of Naij Tal in the Wanbaogou valley, the southern margin of an intrusion is exposed with a porphyritic biotite granite core and a marginal muscorite-tourmaline granite facies (G222, G232). It is unclear on field evidence whether the Wanbaogou granite should be grouped with the three post-tectonic bodies to the south, or with the syn-tectonic Kunlun batholith to the north, but preliminary isotopic data suggest a significantly older intrusive age than either group of intrusions.

The Kunlun batholith, which extends for at least 1000 km along its east–west strike and marks the northern margin of the Tibetan Plateau, is exposed throughout the northern 30 km of the Kunlun Mountains. Along the Geotraverse route its southern expression is the Golmud Hydro granite which has a north–south dimension of 10 km and a minimum east–west extent of 18 km. It is comprised of a biotite granite core (G245) and cut by biotite pegmatites, and aplites. The marginal facies of the intrusion is a strongly porphyritic biotite granite (G244, G260, G261, G263, G264). Both facies are syn-tectonic, contain enclaves of diorite or granodiorite and are cut by abundant mafic dykes. Along the southern contact, the Golmud Hydro granite intrudes andesites and basalts and at the contact the volcanics are strongly hornfelsed and intruded by numerous aplites, quartz veins and granitic dykes. Along the northern contact the granite intrudes a hornblende granodiorite which often shows a pronounced fabric (G249) and an undeformed biotite granodiorite (G248) which is cut by dykes of the porphyritic phase of the Golmud Hydro granite. Five kilometres north of the granodiorite exposures, a biotite–hornblende tonalite (G247) showing local flow-banding forms an actively quarried inlier. The tonalite contains hornblende-rich autoliths and is cut by abundant garnet granite pegmatites.

Along the northern margin of the Kunlun Mountains, plutonic rocks are continuously exposed for several hundred kilometres both east and west of Golmud. Twenty kilometres south-east of Golmud, an active quarry exposes a biotite–hornblende granodiorite (G273, Golmud East). Further east the dominant rock-type is a hornblende–biotite tonalite–granodiorite (G271, G268) which intrudes a strongly foliated biotite granodiorite (G266, Duo Ya He). Apart from abundant basaltic dykes, mafic intrusives are restricted to a single outcrop of norite in this region of the Kunlun batholith.

There are some differences in interpretation amongst authors concerning the sub-division of intrusives in the northern Kunlun Terrane. Jin Chengwei suggests that to the north of the Golmud Hydro granite, a major east–west fault (the Daobangou Fault) separates a northern group of diorites, tonalites and granodiorites (which includes the Duo Ya He and the Golmud East bodies described in this study) from the Central Kunlun (which includes the granites and granodiorites of Golmud Hydro and Wanbaogou). Although not clearly identified along the Geotraverse route, the Daobangou Fault is reported several hundred kilometres to the east, with ultramafic bodies within the fault zone and this fault is identified by Jin Chengwei as a palaeosuture.

PHILOSOPHICAL TRANSACTIONS OF THE ROYAL SOCIETY A MATHEMATICAL, PHYSICAL & ENGINEERING SCIENCES

(*b*) *Geochemistry*

The fabric and field relations of the Kunlun batholith suggests that it may be divided into three facies, the strongly deformed Xidatan granite orthogneiss, the post-tectonic granites and granodiorites of Naij Tal, Xiaonanchuan and Yie Nin Gou, and the syn-tectonic composite batholith ranging from diorite to granite of the northern Kunlun. Geochemically the intrusions can not be categorized in this way (table 3). Major elements indicate that the leucogneiss facies of the Xidatan intrusion is siliceous, calc-alkali syenogranite (figure 16). Despite the high silica content of many samples (> 76 wt. %), modal compositions lie close to the granite eutectic implying a probable magmatic origin. The biotite gneiss from the Xidatan intrusion is similar in composition to the Golmud Hydro syn-tectonic intrusion; they are both monzogranites and lie on the boundary between calc-alkaline and calcic. The Naij Tal post-tectonic granite and the Golmud East and the Duo Ya He syn-tectonic granodiorites are all calcic in composition. There is therefore no obvious spatial or textural correlation with major element geochemistry.

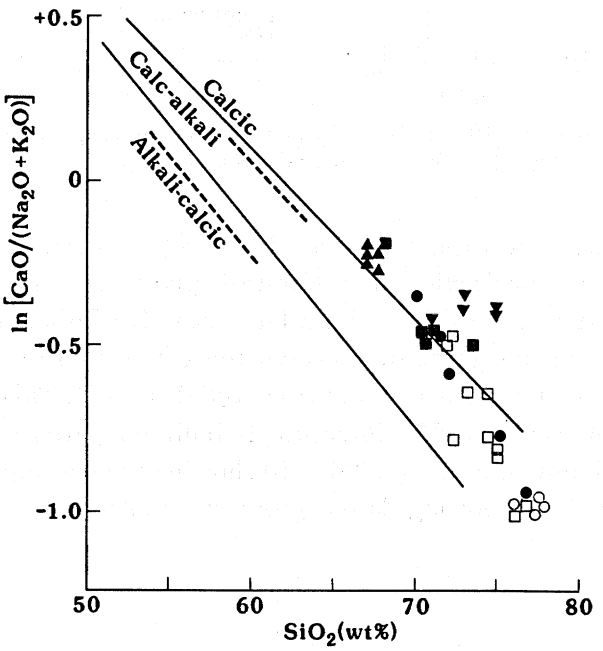

FIGURE 16. Plot of $\log_{10}(CaO/(Na_2O+K_2O))$ against SiO_2 for Kunlun samples. Field boundaries as for figure 3. Data from table 3. ● = Xidatan (biotite gneiss), ○ = Xidatan (leucogneiss), ■ = Naij Tal, □ = Golmud Hydro, ▲ = Golmud East, ▼ = Duo Ya He.

All samples analysed for Rb, Y and Nb lie well within the volcanic arc/post-collision field (figure 17). Granite suites lying in the calcic field of figure 16 often represent island arc magmas (that is volcanic arc magmas generated in the absence of upper crustal contamination) but both Sr and Nd isotopic data require considerable crustal involvement (see Harris, Xu, Lewis, Hawkesworth & Zhang, this volume). Partial melting of a quartz diorite or tonalite parent results in a melt of calcic characteristics (Tindle & Pearce 1983) and such a source is consistent with the Rb/Sr characteristics inferred from Sr–Nd studies. It is likely therefore that melts were

generated at either an active continental margin or in a post-collision setting but the crustal component came from sources of intermediate compositions which were igneous in origin.

The REE from the Kunlun granites fall into two distinct groups. Group A (figure 18*b*) have a high Ce/Yb ratio and a small negative Eu anomaly, as seen in samples from Naij Tal as well as from the Duo Ya He (G266) and Golmud East (G273) facies in the Kunlun batholith. Such

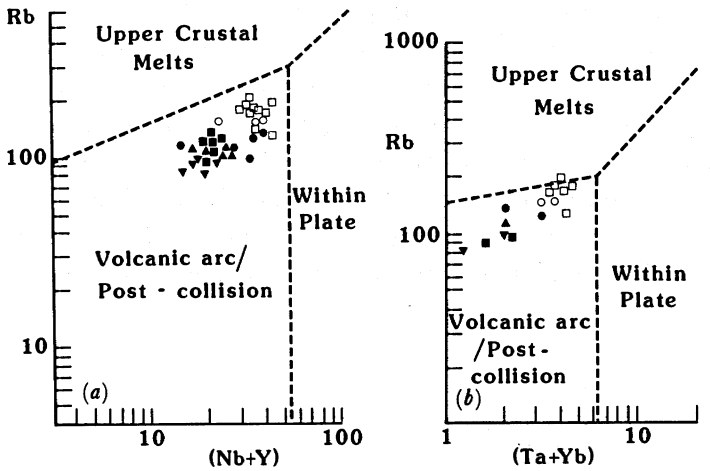

FIGURE 17 (*a*) Rb vs (Nb+Y) plot, (*b*) Rb vs (Ta+Yb) plot for Kunlun samples. Symbols as for figure 16. Field boundaries from Pearce *et al.* (1984).

REE are typical of magmas with a HREE-bearing phase such as garnet in the source, which have undergone limited feldspar fractionation. Group B (figure 18*b*) as seen in the Golmud Hydro intrusion, have flatter patterns but with a large negative Eu anomaly. Such patterns characterize feldspar-bearing but garnet-free crustal sources as seen in the High Himalaya leucogranites (Dietrich & Gansser 1981, Vidal *et al.* 1982) and the Palaeozoic intrusions of the North Himalayas (Debon *et al.* 1986). Interestingly both REE patterns are observed in the Xidatan orthogneiss, the biotite granites (G206A, B) showing steep group A patterns, but the leucogranite gneiss (G206C, D) showing flatter, group B, profiles.

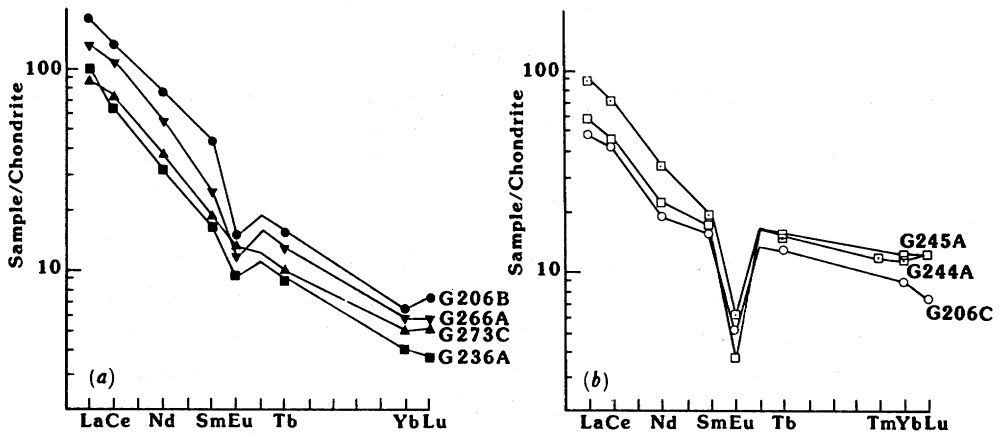

FIGURE 18. Chondrite normalized REE plots for Kunlun samples. (*a*) Group A, Xidatan biotite gneiss (G206B), Naij Tal (G236A), Golmud East (G273C) and Duo Ya He (G266A). (*b*) Group B, Xidatan leucogneiss (G206C) and Golmud Hydro (G244A, G245A).

The two groups can also be clearly distinguished on a Rb/Zr diagram (figure 19). Group B intrusions have elevated Rb/Zr indicative of a crustal source. Group A tend to have lower Rb/Zr than the calc-alkaline Gangdise Belt to the south. This indicates either a low crustal component, as in an island arc setting, or a crustal source of intermediate composition such as a tonalite or amphibolite.

The relationship between these two geochemical groups requires further study, but since they have similar Sr–Nd isotope characteristics in the source (Harris, Xu, Lewis, Hawkesworth

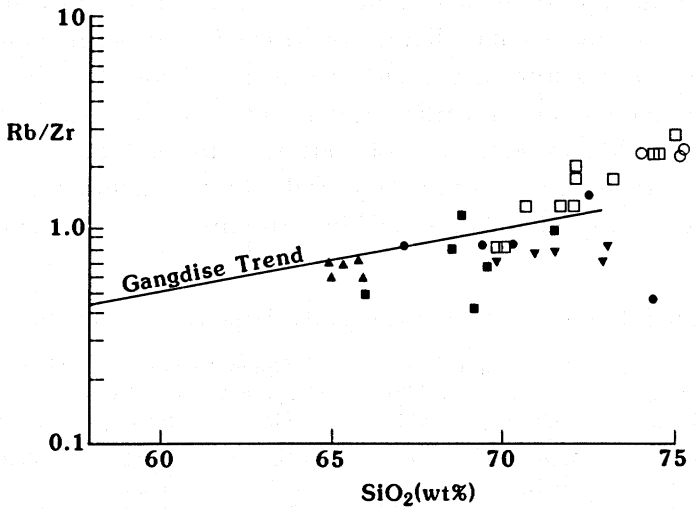

FIGURE 19. Rb/Zr vs SiO_2 for Kunlun samples compared with Gangdise Belt. Symbols as for figure 16. Note that closed symbols represent group A samples and open symbols group B.

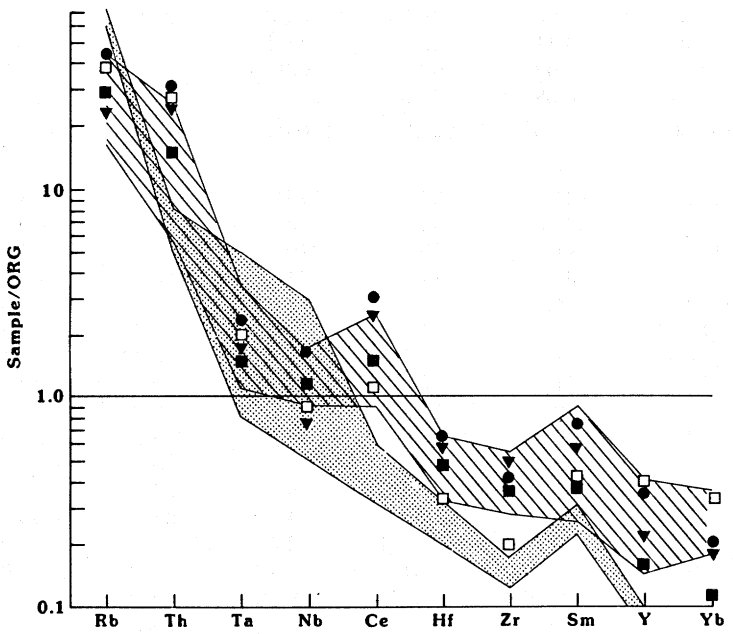

FIGURE 20. Geochemical patterns for granitic samples from Kunlun Terrane (SiO_2 = 71–74 wt. %) normalised against Ocean Ridge Granite (Pearce *et al.* 1984). Lined field = volcanic arc/post-collision granites; stippled field = High Himalayan leucogranites. ● = Xidatan biotite gneiss (G206B), ■ = Naij Tal (G236A), □ = Golmud Hydro (G245A), ▼ = Duo Ya He (G266A).

& Zhang, this volume) it is likely that they are related either by mineral fractionation or by crustal reworking. Although there is a general trend towards higher silica contents in group B intrusions, there is also considerable overlap in the range 72–75 wt. % SiO_2 (see figure 19). It is probable that the group B granites therefore do not result from simple fractionation of feldspar and a LREE-rich phase from a magma of group A geochemistry. If a wide range of trace elements are considered for the Kunlun intrusives (figure 20), the strong depletion of HREE and Y seen in the group A intrusives, and of Zr, Hf seen in group B intrusives indicates probable crustal anatexis. Sr–Nd isotopic constraints in fact require petrogenesis principally from crustal anatexis with only a limited mantle component (Harris, Xu, Lewis, Hawkesworth & Zhang, this volume). Both trace element and isotopic characteristics can be reconciled with a model which derives the group A intrusions from a garnet-bearing crustal source of intermediate composition, and group B from remelting the earlier plutonic suite resulting in predominantly highly siliceous partial melts with low LREE/HREE. Trace elements for both groups indicate either a volcanic arc or a post-collision setting, but the large scale of the batholith requiring a large and long-lived energy source is more characteristic of an active arc than a post-collision setting. A

TABLE 3. SELECTED ANALYSES FROM THE KUNLUN TERRANE

	Xidatan		Naij Tal		Golmud Hydro		Golmud E	Duo Ya He
	G206B Gr gn	G206C Gr gn	G236A Gr	G236D Gd	G245A Gr	G244A por Gr	G273C Gd	G266A Gd
SiO_2	71.40	77.29	73.63	68.07	76.42	74.06	66.97	73.80
TiO_2	0.39	0.08	0.27	0.44	0.04	0.22	0.57	0.37
Al_2O_3	15.30	13.80	14.64	15.73	13.26	13.93	16.31	14.97
Fe_2O_3	2.61	0.84	1.75	2.68	1.13	2.42	3.97	2.49
MnO	0.06	0.03	0.04	0.04	0.04	0.06	0.06	0.03
MgO	0.88	0.15	0.75	1.30	0.18	0.44	1.44	0.83
CaO	2.57	0.93	2.35	3.63	0.83	1.78	4.10	2.91
Na_2O	3.83	3.61	3.96	4.27	3.86	3.92	3.81	3.81
K_2O	3.67	5.04	3.41	2.62	4.62	3.95	3.14	2.54
P_2O_5	0.14	0.08	0.08	0.21	0.04	0.07	0.20	0.12
LOI	0.51	0.11	0.58	0.50	0.40	0.35	0.72	0.06
Total	101.36	101.96	101.46	99.49	100.82	101.20	101.29	101.93
ppm								
Rb	125	152	135	93	178	170	114	102
Sr	300	65	291	492	53	132	500	245
Ba	663	171	711	719	219	767	895	575
Zr	143	63	132	177	74	129	162	136
Hf	5.1	2.6	4.1	4.7	3	3.9	4.6	4.84
Nb	16	16	11	11	9	8.7	9.8	7.9
Ta	1.6	1.6	1.1	0.79	1.5	0.93	0.82	0.58
Y	18	23	11	9	27	29	12	15
Th	23	16	12	11	21	22	12	20
U	1.6	3.2	3.0	3.0	3.0	3.0	4.0	4.0
La	60	13	32	42	19	29	30	44
Ce	114	28	57	73	40	62	64	95
Nd	40	11	20	26	14	22	26	35
Sm	6.6	3	3.4	4.2	3.5	3.9	3.9	5.5
Eu	1.1	0.40	0.74	1.1	0.29	0.70	1.0	0.90
Tb	0.81	0.68	0.49	0.44	0.79	0.84	0.52	0.68
Tm	—	—	—	—	—	0.45	—	0.20
Yb	1.4	2.0	0.91	0.71	2.7	2.7	1.1	1.3
Lu	0.25	0.25	0.13	0.10	0.43	0.43	0.18	0.20

Gr = granite, Gd = granodiorite, por = porphyritic, gn = gneiss.

possible interpretation is that the batholith represents anatexis of garnet amphibolite at intermediate crustal levels above an active continental margin. Some reworking of the igneous suite resulted from convective heat transfer at a destructive margin. The post-tectonic plutons to the south of the batholith are probably younger and were formed in a post-collision setting.

A modification of this model (Jin Chengwei) is that only intrusions along the northern margin of the Kunlun batholith result from active subduction. The Golmud Hydro body is therefore post-collisional in this model, the two groups being separated by a suture zone not clearly identified along the geotraverse route. Along the Golmud–Naj Tal traverse of the Kunlun batholith it is agreed that there is an apparent trend from intrusions of intermediate compositions along the northern margin, to more evolved granitic compositions to the south. However it is the contention of N.B.W.H. that although this could reflect southwards subduction from the north there is no compelling evidence for the location of a suture within the Kunlun Terrane along the geotraverse route.

7. Discussion and conclusions

Three plutonic provinces have been identified in the Tibetan Plateau, each of which can be related to tectonothermal processes at an active, or recently active, plate margin.

The Gangdise Belt is a composite calc-alkaline batholith emplaced along the southern margin of the Lhasa Terrane. Minor gabbroic components within the southern Gangdise Belt with a garnet-bearing, probably mantle source, represent primitive magmas from which more evolved compositions can be derived by fractionation and crustal assimilation. Trace elements are indicative of generation at an active continental margin and the Eocene ages of emplacement (Harris, Xu, Lewis, Hawkesworth & Zhang, this volume) imply formation above a north-dipping subduction zone at the southern margin of the Lhasa Terrane before the Himalayan collision. The northern Gangdise Belt (Nyainqentanglha Mountains) exposes uplifted orthogneisses representing crustal anatexis at deeper crustal levels of the continental margin.

Seven hundred kilometres to the north of the Gangdise Belt, an uplifted granitic batholith forms the northern Kunlun Mountains. This batholith is broadly Permo–Triassic in age (Harris, Xu, Lewis, Hawkesworth & Zhang, this volume) and calcic to calc-alkaline in composition. Trace elements are indicative of formation in a volcanic arc or post-collision setting, but trace element and isotopic constraints require predominantly crustal sources. Magmagenesis can be modelled firstly from anatexis of a garnet-bearing crustal source of intermediate composition, such as a garnet-amphibolite, and secondly by reworking of the earlier-formed plutonic suite. It is postulated that the batholith represents magmagenesis at intermediate crustal depths above an active continental margin prior to and immediately following collision between the Kunlun and Qiangtang terranes.

A belt of Cretaceous tonalite–granite plutons emplaced into the northern Lhasa Terrane constitutes the third plutonic province of the Tibetan Plateau. These form a bimodal suite in which an earlier tonalite–granodiorite component is intruded by peraluminous granite. The bimodal association characterizes post-collision magmagenesis where calc-alkaline magmas are derived from AFC processes above a hydrated mantle wedge and crustal anatexis results from the tectonically thickened crust.

PHILOSOPHICAL TRANSACTIONS OF THE ROYAL SOCIETY A MATHEMATICAL, PHYSICAL & ENGINEERING SCIENCES

The authors thank A. G. Tindle for reconnaissance microprobe data on accessory phases, N. W. Rogers and J. S. Watson for analytical assistance, J. Taylor for drafting the diagrams and M. Leggett for typing the manuscript.

References

Brown, G. C. 1982 Calc-alkaline intrusive rocks: their diversity, evolution and relation to volcanic arcs. In *Andesites* (ed. R. S. Thorpe), pp. 437–461. New York and London: John Wiley and Sons.

Brown, G. C., Thorpe, R. S. & Webb, P. C. 1984 The geochemical characteristics of granitoids in contrasting arcs and comments on magma sources. *J. geol. Soc.* **141**, 411–426.

Chang Chengfa *et al.* 1986 Preliminary conclusions of the Royal Society and Academia Sinica 1985 geotraverse of Tibet. *Nature Lond.* **323**, 501–507.

Debon, F., Le Fort, P., Sheppard, S. M. F. & Sonet, J. 1986 The four plutonic belts of the Transhimalaya-Himalaya: a chemical, mineralogical, isotopic and chronological synthesis along a Tibet-Nepal section. *J. Petrol.* **27**, 219–250.

Debon, F., Le Fort, P., Dantel, D., Sonet, J. & Zimmermann, J. L. 1987 Granites of western Karakorum and northern Kohistan (Pakistan): A composite Mid-Cretaceous to Upper Cenozoic magmatism. *Lithos* **20**, 19–40.

Dietrich, V. & Gansser, A. 1981 The leucogranites of the Bhutan Himalaya. *Schweiz mineral. petrog. Mitt.* **61**, 177–202.

Fourcade, S. & Allègre, C. J. 1981 Trace element behaviour in granite genesis: a case study. The calc-alkaline plutonic association from the Querigut Complex (Pyrenees, France). *Contr. Miner. Petr.* **76**, 177–195.

Harris, N. B. W., Pearce, J. A. & Tindle, A. G. 1986 Geochemical characteristics of collision zone magmatism. In *Collision tectonics* (ed. A. C. Ries & M. P. Coward), *Geol. Soc. Spec. Publ.* **19**, pp. 67–81.

Honnegar, K., Dietrich, V., Frank, W., Gansser, A., Thoni, M. & Trommsdorff, V. 1982 Magmatism and metamorphism in the Ladakh Himalayas (the Indus-Tsangpo suture zone). *Earth planet. Sci. Lett.* **60**, 253–293.

Jin Chengwei & Xu Ronghua 1980 Les Granitoides de la partie centrale de l'Himalaya et du Gangdise au Xizang (Tibet) meridonal. In *Résultats de la co-operation franco-chinoise au Tibet* (ed. J. L. Mercier & Li Guangquin), pp. 289–308.

Peacock, M. A. 1931 Classification of igneous rock series. *J. Geol.* **39**, 54–67.

Pearce, J. A. 1982 Trace element characteristics of lavas from destructive plate boundaries. In *Andesites* (ed. R. S. Thorpe), pp. 525–548. New York and London: J. Wiley and Sons.

Pearce, J. A., Harris, N. B. W. & Tindle, A. G. 1984 Trace element discrimination diagrams for the tectonic interpretation of granitic rocks. *J. Petrol.* **25**, 956–983.

Petterson, M. G. & Windley, B. F. 1985 Rb-Sr dating of the Kohistan arc batholith in the Trans-Himalaya of north Pakistan and tectonic implications. *Earth planet. Sci. Lett.* **74**, 45–57.

Potts, P. J., Thorpe, O. W. & Watson, J. S. 1981 Determination of the REE abundances in 29 international rock standards by Instrumental Neutron Activation Analysis: a critical appraisal of calibration errors. *Chem. Geol.* **34**, 331–352.

Rapp, R. P. & Watson, E. B. 1986 Monazite solubility and dissolution kinetics: implications for the thorium and light rare earth chemistry. *Contr. Miner. Petr.* **94**, 304–316.

Sawka, W. N., Banfield, J. F. & Chappell, B. W. 1986 A weather-related origin of widespread monazite in S-type granites. *Geochim. Cosmochim. Acta* **50**, 171–175.

Streckeisen, A. 1976 To each plutonic rock its proper name. *Earth Sci. Rev.* **12**, 1–33.

Tindle, A. G. & Pearce, J. A. 1983 Assimilation and partial melting of continental crust: evidence from the mineralogy and geochemistry of autoliths and xenoliths. *Lithos* **12**, 185–202.

Vidal, P., Cocherie, A. & Le Fort, P. 1982 Geochemical investigations of the origin of the Manaslu leucogranite (Nepal). *Geochim. cosmochim. Acta* **46**, 2279–2292.

Wickam, S. M. & Oxburgh, E. R. 1986 A rift tectonic setting for Hercynian high-thermal gradient metamorphism in the Pyrenees. *Tectonophysics* **129**, 53–69.

Xu Ronghua, Scharer, U. & Allègre, C. J. 1985 Magmatism and metamorphism in the Lhasa Block (Tibet): a geochronological study. *J. Geol.* **93**, 41–57.

PHILOSOPHICAL TRANSACTIONS OF THE ROYAL SOCIETY A MATHEMATICAL, PHYSICAL & ENGINEERING SCIENCES

PHILOSOPHICAL TRANSACTIONS OF THE ROYAL SOCIETY A MATHEMATICAL, PHYSICAL & ENGINEERING SCIENCES

H

HARRIS, XU, LEWIS & JIN

Appendix. Geochemical analyses of granitic rocks from the Tibetan Plateau

1 = Analysed at Open University England. Majors from XRF discs (all Fe calculated as Fe_2O_3), traces from XRF pellets and INAA.

2 = Analysed at Institute of Geology, Beijing (Academia Sinica). Majors from wet chemistry, traces from ICP.

Locality:	S. Lhasa Terrane									
	Quxu			Lhasa	Dagze	Yangbajain		Nyainqentanglha		
	G4[1]	G5[1]	G10[1]	G12[1]	G15A[1]	G20[1]	G26[1]	G38E[1]	G40[1]	G41B[1]
SiO_2	58.73	61.00	73.76	65.96	60.00	74.25	69.30	73.22	72.12	71.76
TiO_2	0.71	0.70	0.22	0.75	0.83	0.19	0.43	0.37	0.29	0.35
Al_2O_3	17.18	16.85	14.20	15.41	16.86	14.14	15.77	12.43	14.68	14.60
Fe_2O_3	6.97	5.61	1.73	4.98	7.24	1.31	2.99	1.97	2.20	2.57
FeO										
MnO	0.13	0.10	.03	0.07	0.14	0.08	0.09	0.03	0.03	0.06
MgO	2.82	2.63	0.61	1.56	2.80	0.12	0.98	0.60	0.45	.80
CaO	6.15	5.34	1.71	4.17	5.74	1.02	2.54	1.46	1.32	2.03
Na_2O	3.99	4.25	3.00	3.44	3.92	3.43	4.20	2.84	3.27	3.64
K_2O	2.55	3.27	5.53	3.16	1.84	5.18	4.66	4.88	5.67	4.50
P_2O_5	0.20	0.28	0.05	0.18	0.23	0.00	0.15	0.10	0.09	0.08
H_2O^+										
H_2O										
Loss	0.35	0.32	0.21	0.61	0.33	0.21	0.51	0.29	0.44	0.29
Total	99.78	100.35	101.05	100.29	99.93	99.93	101.63	98.19	100.56	100.68
Rb	58	110	137	108	57	229	174	220	331	240
Sr	645	867	242	304	470	152	368	345	224	180
Ba	623	660	370	620	381	358	886	<250	480	630
Zr	127	174	99	208	101	119	190	147	225	133
Hf					3.9	3.8	5.5			
Nb	6	13	3	7	7	13	10	25	10	11
Ta					0.44	1.6	1.2			
Y	19	18	5	36	20	30	24	13	22	24
Th	6	27	21	6	4.0	21	17	78	73	28
U	<3	6	4	<3	0.97	3.0	3.4	5	<4	<4
La					21	34	53			
Ce					41	69	101			
Nd			14		21	26	36			
Sm			1.7		4.3	5.6	6.0			
Eu					1.2	0.77	1.3			
Tb					0.68	0.89	0.75			
Tm					0.34	0.52	0.36			
Yb					2.1	3.3	2.8			
Lu					0.34	0.46	0.42			

PHILOSOPHICAL TRANSACTIONS OF THE ROYAL SOCIETY A MATHEMATICAL, PHYSICAL & ENGINEERING SCIENCES

					N. Lhasa Terrane Bamang Co.			Baingoin		
	G42A[1]	G42B[1]	S70C[1]	S70D[1]	G66A[2]	G67A[1]	X45[1]	G68A[1]	G68B[2]	G69A[1]
SiO_2	72.33	71.35	76.05	72.87	70.09	66.84	65.60	64.27	71.80	77.41
TiO_2	0.31	0.32	0.11	0.26	0.46	0.43	0.46	0.53	0.20	0.05
Al_2O_3	15.46	14.74	13.75	14.52	14.21	15.89	15.80	16.62	14.88	12.44
Fe_2O_3	2.06	1.97	1.25	1.79	0.00	4.16	4.41	5.19	0.00	0.54
FeO					3.42				1.58	
MnO	0.03	0.04	0.02	0.04	0.06	0.09	0.10	0.10	0.0	0.02
MgO	0.39	0.32	0.18	0.31	0.78	1.46	1.83	2.43	0.71	0.14
CaO	1.64	1.41	0.89	1.44	2.01	4.09	4.22	5.21	1.5	0.69
Na_2O	3.60	3.31	3.29	3.67	2.96	2.66	2.84	2.55	3.04	2.35
K_2	5.53	5.72	5.71	4.81	5.0	3.30	3.30	2.34	5.51	5.95
P_2O_5	0.08	0.06	0.13	0.08	0.17	0.11	0.08	0.13	0.09	0.07
H_2O^+					0.60				0.58	
H_2O^-					0.02				0.06	
Loss	0.26	0.25	0.37	0 .33	0.34	0.61	0 .56	0.75	0.23	0.50
Total	101.59	99.49	101.75	100.12	100.13	99.64	99.20	100.12	100.26	99.71
Rb	236	319	339	264		168	174	130		296
Sr	303	302	127	236	110	296	300	301	115	62
Ba	330	660	<210	750	230	<290	370	<310	459	<190
Zr	225	241	118	175	88	119	127	126	310	51
Hf	6.9	5.3	4.2							
Nb	8	14	17	10	12	12	10	6		
Ta	3.0	.92	.98							
Y	14	8	25	18	26	24	26	42	40	18
Th	73	52	55	43		17	22	7.3		8
U	8.9	<4	31	6.3		<4	<4	3.1		4
La	90			54	27			19	57	
Ce	167			108				40		
Nd	54		38	38				23		
Sr	7.2		8.1	6.3				6.2		
Eu	1.0			0.83				1.1		
Tb	1.1			0.95				1.2		
Tm										
Yb	1.5			1.6				3.9		
Lu	0.25			0.25				0.58		

PHILOSOPHICAL TRANSACTIONS OF THE ROYAL SOCIETY A MATHEMATICAL, PHYSICAL & ENGINEERING SCIENCES

Pang Co

	G69C[2]	G71[1]	G100A[1]	G100C[1]	G100E[2]	G101A[1]	G101C[2]	G101E[2]	G101G[1]
SiO_2	76.79	71.49	74.52	73.01	75.48	58.74	58.33	58.51	59.40
TiO2	0.05	0.32	0 .30	0.28	0.26	0.81	0.74	0.85	0.76
Al2O3	12.17	15.57	13.99	14.85	12.12	15.75	15.57	15.39	15.60
Fe_2O_3	0.00	3.24	1.53	1.49	0.66	7.45	1.94	1.79	7.04
FeO	0.91				1.28		4.77	4.92	
MnO	0.02	0.07	0.03	0.04	0.04	0.12	0.11	0.12	0.11
MgO	0.19	1.08	0.30	0.45	0.32	4.07	4.01	3.98	4.03
CaO	0.75	1.63	.94	1.20	0.54	6.49	6.40	6.31	6.22
Na_2O	1.95	2.85	3.07	3.75	2.82	3.02	2.88	2.91	2.64
K_2O	6.29	4.41	5.44	5.35	5.80	2.94	2.94	3.01	2.98
P_2O_5	0.09	0.17	0.05	0.06	0.04	0.20	0.15	0.15	0.19
H_2O^+	0.28				0.06		1.02	0.91	
H_2O^-	0.00				0.09		0.31	0.35	
Loss	0.14	0.88	0.42	0 .51	0.28	0.64	0.37	0.33	0.65
Total	99.63	101.71	100.59	100.99	99.76	100.23	99.54	99.53	99.62

Rb	391	303	348	169	72				
Sr	64	112	104	128	149	310	278	278	295
Ba	152	<270	<250	<260	493	350	399	414	710
Zr	61	119	165	182	230	200	200	210	245
Hf		3.7							
Nb		16	13	18		10			10
Ta		2.7							
Y	14	21	24	39	27	29	22	24	28
Th		17	55	62		25			25
U		2.9	<4	4		<4			4
La	<10	29			68		43	46	
Ce		61							
Nd		27							
SM		5.4							
Eu		0.74							
Tb		0.75							
Tm									
Yb		1.36							
Lu		0.23							

	Nyainrong					Amdo				
	G57A[2]	G60A[1]	G61A[1]	G64A	G64C[1]	G120A[2]	G121B[2]	G124A[1]	G124C[1]	G125A[2]
SiO_2	73.52	68.98	70.00	71.56	70.75	70.25	62.45	62.28	62.86	63.15
TiO_2	0.18	0.58	0.46	0.39	0.51	0.23	0.59	0.79	0.82	0.70
Al_2O_3	13.81	14.01	14.18	14.76	15.54	15.22	17.19	16.74	16.99	16.33
Fe_2O_3	0.70	3.14	2.62	2.16	2.72	0.00	0.03	5.49	5.87	0.00
FeO	1.08					2.01	4.58			5.01
MnO	0.05	0.06	0.06	0.04	0.04	0.07	0.10	0.09	0.10	0.09
MgO	0.26	2.05	1.54	0.50	0.69	1.00	2.60	2.76	2.66	2.51
CaO	0.89	2.59	2.23	2.02	2.13	2.25	5.80	4.42	3.86	3.69
Na_2O	2.86	2.84	2.39	3.28	2.95	3.67	3.13	3.89	3.13	3.21
K_2O	5.58	5.20	5.61	4.89	5.27	4.14	1.87	3.07	3.40	3.52
P_2O_5	0.15	0.20	0.17	0.10	0.18	0.06	0.10	0.16	0.19	0.20
H_2O^+	0.48					0.42	0.83			1.01
H_2O^-	0.08					0.18	0.29			0.25
Loss	0.29	0.80	1.33	0.57	0.57	0.46	0.46	0.88	0.84	0.17
Total	99.93	100.45	100.59	100.27	101.35	99.96	100.02	100.57	100.72	99.84
Rb	319	325	353	387				198	204	
Sr	64	272	221	227	276	167	254	262	269	207
Ba	484	80	532	<280	540	717	387	450	770	766
Zr	140	300	236	246	292	167	130	212	238	290
Hf				6.8				6.7		
Nb		19	15	19	24			16	15	
Ta				1.3				1.7		
Y	26	26	19	14	27	21	20	35	36	21
Th		50	46		86			14	26	
U		<4	<4		6			7	<4	
La	45			90		36	19	25		71
Ce				147				52		
Nd				48				29		
Sm				9.2				6.6		
Eu				.97				1.4		
Tb				1.1				1.0		
Tm										
Yb				1.3				2.9		
Lu				0.19				0.49		

PHILOSOPHICAL TRANSACTIONS OF THE ROYAL SOCIETY A MATHEMATICAL, PHYSICAL & ENGINEERING SCIENCES

	Mo Tian Ling					Amdo Basement				
	G111B[1]	G111C[2]	G111D[1]	G112A[1]	G114B[1]	G115A[1]	G115B[1]	G117A[1]	G117B[1]	G118A[1]
SiO_2	66.21	64.51	63.54	52.23	71.77	68.43	66.44	47.28	47.23	68.98
TiO_2	0.71	0.72	0.80	0.90	0.40	0.57	0.59	1.22	1.09	0.43
Al_2O_3	16.91	16.25	16.79	14.90	15.15	15.99	16.31	15.79	14.76	14.86
Fe_2O_3	3.76	0.48	4.25	8.22	2.15	3.16	3.50	10.95	10.34	4.53
FeO		3.09								
MnO	0.06	0.07	0.07	0.13	0.04	0.06	0.06	0.13	0.20	0.08
MgO	1.72	1.71	1.88	8.73	.85	1.49	1.87	6.54	6.70	1.47
CaO	3.48	3.53	3.80	7.79	2.06	2.93	3.86	11.12	14.79	3.30
Na_2O	4.26	4.31	4.35	2.83	3.65	4.06	3.99	3.20	1.87	3.74
K_2O	3.55	3.54	3.47	1.86	4.82	3.75	2.97	0.92	0.80	1.54
P2O5	0.21	0.22	0.23	0.21	0.13	0.16	0.17	0.12	0.14	0.10
H_2O^+		0.59								
H_2O^-		0.20								
Loss	0.52	0.15	0.59	2.34	0.34	0.47	0.63	0.52	0.84	0.76
Total	101.39	99.37	99.77	100.14	101.36	101.07	100.39	97.89	98.76	99.79
Rb	159		156	103	156	201	146			
Sr	364	318	387	311	223	287	374	19	38	140
Ba	550	615	580	780	320	340	670	140	151	168
Zr	226	310	255	116	145	171	151	<370	<370	410
Hf			5.9	2.9	3.8			84	79	156
Nb	16		18	9						
							16	16	12	
Ta			1.5	0.60	2.5			10	11	11
Y	20	19	25	21	28	24	17			
Th	25		27	5.6	37	26	16	29	30	22
U	<4		3.2	1.1	2.4	<4	<4	<3	<3	17
La		52	64	19	34					
Ce			114	39	65					
Nd			39	20	29	28				
Sm			6.5	4.3	5.9	5.2				
Eu			1.5	1.2	0.93					
Tb			0.92	0.61	1.2					
Tm										
Yb			2.4	2.0	2.5					
Lu			3.8	0.30	0.38					

	Qiangtang Terrane								S. Kunlun Terrane	
				Mt. Munai (boulders)		Fenguoshan			Wudaoliang	
	G118C[1]	G118D[1]	G118G[1]	G136A[2]	G136B[2]	G141A[1]	G141B[1]	G141D[2]	G142A[1]	G142B[1]
SiO	70.85	69.91	68.74	59.61	70.11	60.58	61.07	59.15	63.09	63.86
TiO_2	0.37	0.41	0.46	0.80	0.31	0.46	0.45	0.43	0.62	0.59
Al_2O_3	15.17	15.34	15.48	15.80	14.80	14.45	14.77	14.33	14.76	15.19
Fe_2O_3	3.69	3.87	4.64	0.16	0.36	4.10	3.78	1.86	6.50	6.28
FeO				4.65	1.83			2.24		
MnO	0.08	0.08	0.08	0.08	0.05	0.08	0.06	0.05	0.16	0.16
MgO	1.24	1.25	1.54	3.74	0.92	1.40	1.62	1.38	3.38	3.41
CaO	2.97	3.05	3.44	5.64	2.03	4.45	4.19	4.90	6.69	6.64
Na_2O	5.03	4.39	4.20	3.78	3.58	3.71	4.01	3.14	1.92	1.99
K_2O	1.33	1.39	1.61	4.09	5.01	5.69	5.86	6.58	1.62	1.61
P_2O_5	0.05	0.08	0.14	0.42	0.18	0.35	0.36	0.41	0.09	0.10
H_2O^+				0.20	0.21			0.90		
H_2O^-				0.28	0.17			0.42		
Loss	0.36	0.39	0.44	0.09	0.11	3.96	3.52	3.28	0.91	0.86
Total	101.14	100.16	100.77	99.34	99.67	99.23	99.69	99.07	99.74	100.69
Rb	125	129	147						65	66
Sr	128	137	175	1328	512	3694	3750	3678	238	243
Ba	<270	<280	490	1666	851	3842	3441	3430	480	430
Zr	154	137	153	295	170	238	233	250	131	132
Hf										
Nb	14	14	11			12	11		10	10
T										
Y	17	23	17	21	18	14	12	11	22	21
Th	9	14	19			20	22		6	6
U	<3	<3	<3			12	14		<3	<3
La				82	61			85		
Ce										
Nd										
Sm										
Eu										
Tb										
Tm										
Yb										
Lu										

PHILOSOPHICAL TRANSACTIONS OF THE ROYAL SOCIETY A MATHEMATICAL, PHYSICAL & ENGINEERING SCIENCES

			Kunlun Pass (boulders)		Xidatan					
	G142D[1]	G143A[1]	G204B[2]	G204D[2]	G206A[1]	G206B[1]	G206C[1]	G206D[1]	G206E[1]	G207[1]
SiO_2	63.75	75.56	70.45	73.19	76.40	71.40	77.29	77.30	76.11	74.54
TiO_2	0.59	0.11	0.31	0.22	0.08	0.39	0.08	0.10	0.90	0.16
Al_2O_3	15.13	14.14	15.47	14.00	13.67	15.30	13.80	13.37	13.32	14.44
Fe_2O_3	6.46	0.68	0.00	0.13	0.84	2.61	0.84	0.84	0.65	1.14
FeO			2.35	1.61						0.00
MnO	0.16	0.01	0.05	0.08	0.03	0.06	0.03	0.03	0.02	0.03
MgO	3.63	0.19	0.72	0.51	0.15	0.88	0.15	0.15	0.25	0.28
CaO	6.54	1.84	2.71	0.95	0.92	2.57	0.93	0.88	0.87	1.43
Na_2O	2.23	2.53	3.87	3.14	3.46	3.83	3.61	3.64	3.86	3.48
K_2O	1.62	5.02	2.85	4.66	4.92	3.67	5.04	4.93	4.86	5.18
$P2O_5$	0.11	0.05	0.13	0.21	0.03	0.14	0.08	0.07	0.04	0.07
H_2O^+			0.80	0.72						
H_2O^-			0.00	0.02						
Loss	0.80	0.39	0.04	0.00	0.44	0.51	0.11	0.27	0.66	0.41
Total	100.30	100.52	99.75	99.44	100.94	101.38	101.96	101.58	101.54	101.16
Rb	66	119			99	125	152	155	156	115
Sr	232	177	381	85	495	300	65	62	71	150
Ba	350	398	896	369	1023	663	171	193	228	283
Zr	128	77	190	158	253	143	63	65	64	76
Hf					6.9	5.1	2.6	2.8		
Nb	8	8			18	16	16	14	11	9
Ta					0.96	1.6	1.6	1.5		
Y	20	7	9	22	14	18	23	16	11	5
Th	5	16			19	23	16	15		
U	<3	3			4.0	1.6	3.2	2.6	15	6
La			36	27	79	60	13	14	3	3
Ce					154	114	28	29		
Nd					48	40	11	11		
Sm					7.1	6.6	3.0	2.8		
Eu					1.7	1.1		0.40	0.40	
Tb					0.75	0.81	0.68	0.56		
Tm					.26					
Yb					1.2	1.4	2.0	1.7		
Lu					0.21	0.25	0.25	0.25		

PHILOSOPHICAL TRANSACTIONS OF THE ROYAL SOCIETY A MATHEMATICAL, PHYSICAL & ENGINEERING SCIENCES

		Xiaonanchuan		Yie Nin Gou		Naij Tal			
	G208[1]	G214A[2]	G214D[2]	G221A[2]	G221J[2]	G236A[1]	G236D[1]	G236E[1]	G236F[1]
SiO_2	72.34	69.24	75.69	67.23	68.67	73.63	68.07	70.66	71.78
TiO_2	0.33	0.39	0.05	0.48	0.47	0.27	0.44	0.30	0.32
Al_2O_3	14.95	15.39	13.31	15.88	15.75	14.64	15.73	14.66	15.70
Fe_2O_3	2.34	0.00	0.18	0.00	0.00	1.75	2.68	1.85	1.97
FeO		2.57	0.59	2.77	2.90				
MnO	0.06	0.05	0.05	0.06	0.05	0.04	0.04	0.04	0.04
MgO	0.70	0.92		1.19	1.08	0.75	1.30	0.87	0.74
CaO	2.02	2.65	0.91	3.41	3.22	2.35	3.63	2.49	2.55
Na_2O	3.82	4.08	4.08	4.47	4.49	3.96	4.27	3.99	4.40
K_2O	4.01	3.46	4.35	2.90	2.93	3.41	2.62	3.60	3.71
P_2O	0.17	0.14	0.01	0.22	0.20	0.08	0.21	0.12	0.13
H_2O^+		0.55	0.12	0.49	0.31				
H_2O^-		0.00	0.00	0.00	0.00				
Loss	0.56	0.18	0.25	0.49	0.25	0.58	0.50	0.33	0.40
Total	101.30	99.62	99.59	99.57	100.31	101.46	99.49	98.91	101.74
Rb	136					135	93	119	135
Sr	271	528	34	550	507	291	492	327	342
Ba	628	918		815	793	711	719	842	687
Zr	153	260	96	225	217	132	177	140	141
Hf						4.1	4.7		
Nb	19					11	11	10	11
Ta						1.1	0.79		
Y	18	9	4	9	9	11	9	9	10
Th	18					12	11	12	12
U	3					3.0	3.0	3	3
La		62	<10	48	47	32	42		
Ce						57	73		
Nd						20	26	20	
Sm						3.4	4.2	3.4	
Eu						0.74	1.1		
Tb						0.49	0.44		
Tm									
Yb						0.91	0.71		
Lu						0.13	0.10		

PHILOSOPHICAL TRANSACTIONS OF THE ROYAL SOCIETY A MATHEMATICAL, PHYSICAL & ENGINEERING SCIENCES

	Wanbaugou					Golmud Hydro				
	G236G[1]	G237[1]	G222A[2]	G222C[2]	G222D[2]	G244A[1]	G244B[1]	G245A[1]	G245B[1]	G245C
SiO_2	71.60	71.15	70.00	70.35	73.19	74.06	73.75	76.42	77.01	76.67
TiO_2	0.33	0.38	0.44	0.34	0.25	0.22	0.20	0.04	0.05	0.04
Al_2O_3	16.15	15.43	13.66	14.20	13.57	13.93	14.03	13.26	13.67	13.35
Fe_2O_3	2.08	2.60	0.00	0.00	0.00	2.42	2.40	1.13	1.13	1.17
FeO			4.69	3.24	2.54					
MnO	0.04	0.06	0.06	0.05	0.06	0.06	0.06	0.04	0.05	0.04
MgO	0.92	1.01	0.61	0.47	0.48	0.44	0.50	0.18	0.22	0.15
CaO	2.78	2.55	2.06	1.90	2.01	1.78	1.76	0.83	0.86	0.83
Na_2O	4.57	3.79	3.59	3.70	4.18	3.92	3.82	3.86	3.60	3.87
K_2O	3.46	3.58	3.99	4.37	3.03	3.95	3.92	4.62	4.77	4.52
P_2O_5	0.12	0.14	0.14	0.10	0.08	0.07	0.05	0.04	0.09	0.05
H_2O^+			0.50	0.87	0.39					
H_2O^-			0.04	0.10	0.07					
Loss	0.49	0.52	0.37	0.55	0.02	0.35	0.50	0.40	0.40	0.21
Total	102.54	101.21	100.15	100.24	99.87	101.20	100.97	100.82	101.85	100.90
Rb	123	103				170	174	178	181	175
Sr	381	535	123	125	171	132	139	53	58	52
Ba	891	817	387	526	627	767		219	294	228
Zr	158	222	312	265	160	129	132	74	63	72
Hf					3.9		3.0	2.6		
Nb	11	11			9	8	9	9	9	
Ta						0.93		1.5	1.6	
Y	10	12	36	37	14	29	26	27	23	28
Th	11	13				22	18	21	18	21
U	3	3			3.0	3	3.0	2.7	3	
La			64	54	34	29		19	19	
Ce						62		40	36	
Nd						22		14	13	
Sm						3.9		3.5	3.1	
Eu						0.70		0.29	0.32	
Tb						0.84		0.79	0.66	
Tm						0.45				
Yb						2.7		2.7	2.6	
Lu						0.43		0.43	0.36	

	G245E[1]	G245F[1]	G246A[2]	G248A[2]	G249D[2]	G260E[1]	G261B[1]	G263A[1]	G247[2]	Golmud East G273A[1]
SiO_2	75.33	74.25	68.28	73.01	68.40	72.08	71.93	74.21	65.76	66.96
TiO_2	0.10	0.90	0.38	0.15	0.34	0.31	0.33	0.16	0.50	0.58
Al_2O_3	13.35	13.53	15.90	13.83	15.28	14.37	14.33	13.95	16.62	16.41
Fe_2O_3	1.63	1.64	0.00	0.00	0.00	3.54	3.52	2.03	0.16	3.95
FeO			3.36	2.23	3.59				3.44	
MnO	0.06	0.06	0.09	0.06	0.09	0.07	0.08	0.05	0.09	0.06
MgO	0.15	0.26	0.89	0.25	0.53	0.75	0.77	0.21	1.23	1.58
CaO	1.21	1.20	3.95	1.63	2.93	2.46	2.41	1.40	4.56	4.24
Na_2O	3.91	4.16	4.34	3.59	4.45	3.65	4.14	3.75	3.97	3.71
K_2O	4.19	4.25	1.30	4.25	3.09	3.37	3.08	4.67	1.68	2.85
P_2O_5	0.03	0.03	0.16	0.07	0.09	0.08	0.08	0.06	0.17	0.20
H_2O^+			0.28	0.18	0.46				0.43	
$H2O^-$			0.00	0.00	0.14				0.00	
Loss	0.22	0.61	0.56	0.27	0.07	0.68	0.54	0.48	1.13	0.66
Total	100.18	100.89	99.49	99.52	99.46	101.36	101.21	100.97	99.74	101.20
Rb	177	183				137	132	200		104
Sr	111	105	528	137	207	180	182	92	616	504
Ba	665	624	381	530	606		744	555	564	826
Zr	95	92	238	150	383	167	162	117	193	163
Hf		3.2					5.0	3.6		
Nb	9	10				12	11	8		11
Ta		1.2					1.1	.69		
Y	21	25	8	17	27	26	30	24	8	15
Th	19	21				23	23	28		11
U	6	5.0				3	3.0	3.7		3
La		27	32	35	88		35	32	39	
Ce		54					72	63		
Nd		18					26	21		
Sm		4.0					5.2	4.4		
Eu		0.47					0.84	0.54		
Tb		0.79					0.96	0.75		
Tm		0.40					0.46			
Yb		2.6					3.1	2.3		
Lu		0.43					0.48	0.38		

PHILOSOPHICAL TRANSACTIONS OF THE ROYAL SOCIETY A MATHEMATICAL, PHYSICAL & ENGINEERING SCIENCES

	G273B[1]	G273C[1]	G273D[1]	G273E[1]	G266A[1]	G266C[1]	G266D[1]	G266E[1]	G268D[2]	G271A[2]
SiO_2	67.34	66.97	67.73	66.80	73.81	74.94	75.23	73.67	67.70	64.75
TiO_2	0.52	0.57	0.54	0.58	0.37	0.25	0.21	0.31	0.40	0.70
Al_2O_3	16.22	16.31	15.97	16.34	14.97	14.23	14.58	14.58	15.14	15.10
Fe_2O_3	3.70	3.97	3.62	4.25	2.49	1.71	1.59	2.11	0.19	0.00
FeO									3.12	6.17
MnO	0.06	0.06	0.06	0 .07	0.03	0.03	0.03	0.03	0.07	0.11
MgO	1.49	1.44	1.42	1.68	0.83	0.65	0.53	0.80	1.38	1.77
CaO	3.98	4.10	3.87	4.23	2.91	2.52	2.62	2.70	3.90	4.77
Na_2O	3.76	3.81	3.73	3.86	3.81	3.66	4.14	3.88	3.33	3.41
K_2O	3.18	3.14	3.45	2.96	2.54	2.75	2.33	2.71	2.94	1.79
P_2O_5	0.20	0.20	0.17	0 .20	0.12	0.08	0.06	0.08	0.14	0.15
H_2O^+									0.68	0.74
H_2O^-									0.04	0.69
Loss	0.20	0.72	0.70	0.64	0.60	0.51	0.49	0.50	0.41	0.16
Total	101.11	101.29	101.26	101.61	102.48	101.33	101.81	101.41	99.44	100.21
Rb	112	114	115	108	102	94	99	82		
Sr	491	500	487	484	245	228	233	218	423	226
Ba	911	895	1005	813	575	539	600	505	606	376
Zr	160	162	155	173	136	128	115	97	133	184
Hf		4.6			4.8					
Nb	8	10	10	9	8	5	7	6		
Ta			0.82		0.58					
Y	9	12	13	11	15	13	12	13	11	21
Th	10	12	12	9	20	20	13	11		
U	3	4.0	4	3	4.0	3	3	3		
La			30		44				30	27
Ce			64		95					
Nd			26		35			29		
Sm			3.9	3.8	5.5			4.9		
Eu			1.0		0.90					
Tb			0.52		0.68					
Tm					0.20					
Yb			1.1		1.3					
Lu			0.18		0.20					

PHILOSOPHICAL TRANSACTIONS OF THE ROYAL SOCIETY A MATHEMATICAL, PHYSICAL & ENGINEERING SCIENCES